Rictor/mTORC2 Loss in the Myf5 Lineage Reprograms Brown Fat Metabolism and Protects Mice against Obesity and Metabolic Disease

Graphical Abstract
Click here to download high resolution image

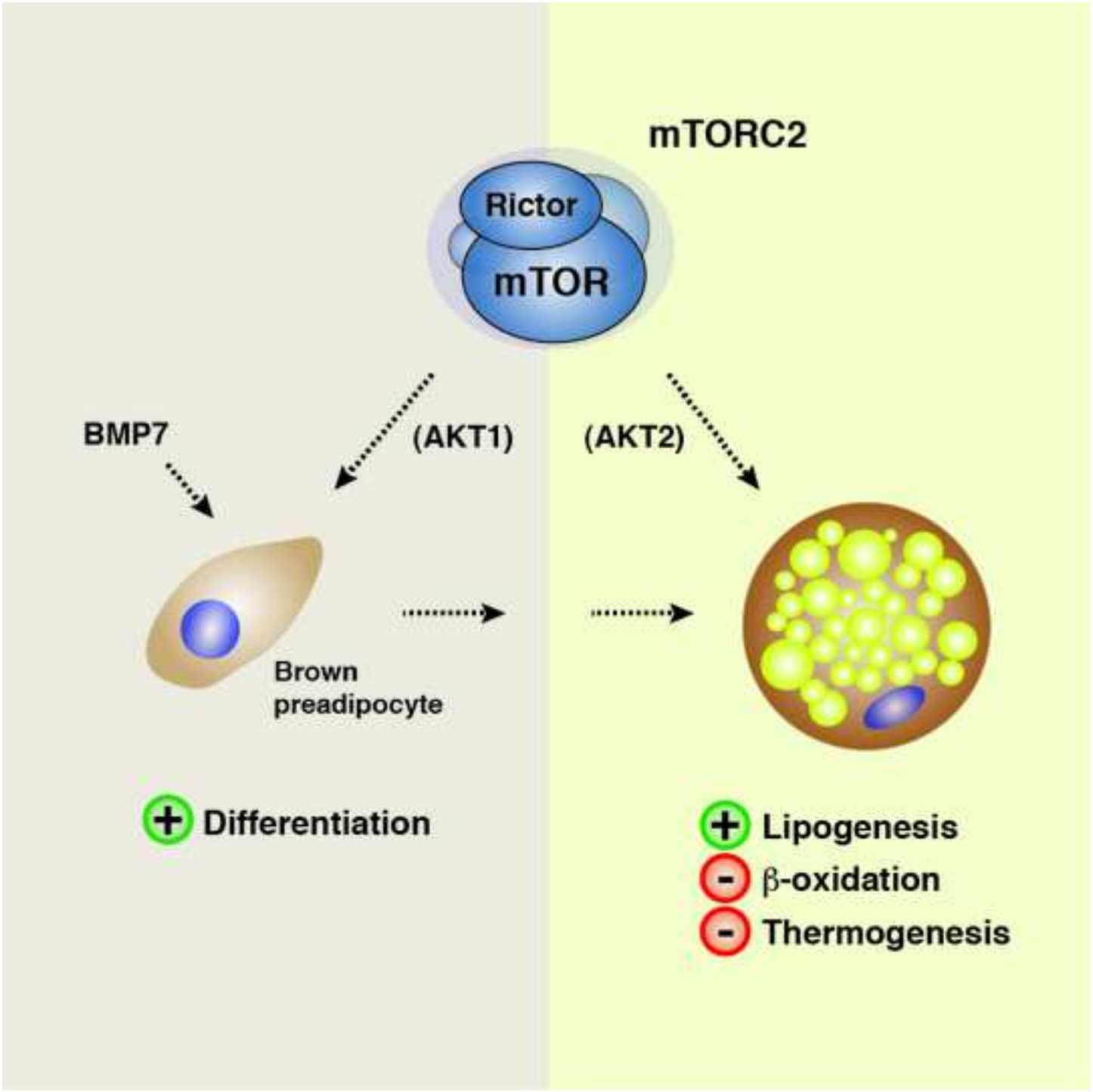

HIGHLIGHTS

- Brown and white adipocyte growth requires mTORC2
- mTORC2 promotes lipogenesis and suppresses β-oxidation in brown fat
- Brown preadipocytes also require mTORC2 to differentiate in vitro
- Inhibiting mTORC2 in BAT enhances diet-induced thermogenesis

Rictor/mTORC2 Loss in the *Myf5*-lineage Reprograms Brown Fat Metabolism and Protects Mice against Obesity and Metabolic Disease

Chien-Min Hung[1], Camila Martinez Calejman[1], Joan Sanchez-Gurmaches[1], Huawei Li[1], Clary B. Clish[2], Simone Hettmer[3,4,5,7,8], Amy J. Wagers[3,4,5,6], and David A. Guertin[1]*

[1]Program in Molecular Medicine, University of Massachusetts Medical School, Worcester, MA 01605, USA
[2]Broad Institute, Cambridge, Massachusetts, USA 02142
[3]Howard Hughes Medical Institute
[4]Department of Stem Cell and Regenerative Biology, Harvard Stem Cell Institute, 7 Divinity Avenue, Cambridge, MA 01238, USA
[5]Joslin Diabetes Center, One Joslin Place, Boston, MA 02215, USA
[6]Department of Cell Biology, Harvard Medical School, Boston, MA 02155, USA
[7]Department of Pediatric Oncology, Dana Farber Cancer Institute, Boston, MA 02155
[8]Division of Pediatric Hematology/Oncology, Children's Hospital, Boston, MA 02155

*Correspondence: david.guertin@umassmed.edu
Contact Information
Phone: 508-856-8065
Fax: 508-856-4289

Running Title: mTORC2 regulates brown adipocyte function

Summary

The in vivo functions of mTORC2, and the signaling mechanisms that control brown adipose tissue (BAT) fuel utilization and activity, are not well understood. Here, by conditionally deleting *Rictor* in the *Myf5*-lineage, we provide in vivo evidence that mTORC2 is dispensable for skeletal muscle development and regeneration but essential for BAT growth. Furthermore, deleting *Rictor* in *Myf5* precursors shifts BAT metabolism to a more oxidative and less lipogenic state and protects mice from obesity and metabolic disease at thermoneutrality. We additionally find that Rictor is required for brown adipocyte differentiation in vitro, that the mechanism specifically requires AKT1 hydrophobic motif phosphorylation but is independent of pan-AKT signaling, and is rescued with BMP7. Our findings provide new insights into the signaling circuitry that regulates brown adipocytes and could have important implications for developing therapies aimed at increasing energy expenditure as a means to combat human obesity.

Introduction

Adipose tissue is essential for many biological processes and its dysfunction, for example in obesity, is associated with a growing spectrum of human diseases. Thus, understanding the developmental and metabolic regulation of adipose tissue has broad clinical implications. There are two main classifications of adipose tissue based on histological appearance: white adipose tissue (WAT) and brown adipose tissue (BAT). WAT is the major energy storage site in the body and has critical endocrine functions (Gesta et al., 2007) while BAT dissipates energy as heat in a process called nonshivering thermogenesis (Cannon and Nedergaard, 2004). BAT is particularly important in small rodents and newborn humans to defend against cold exposure and its functional relevance in adult humans was only recently appreciated (Cypess et al., 2009; Nedergaard et al., 2007; van Marken Lichtenbelt et al., 2009; Virtanen et al., 2009). Brown adipocytes are thermogenic because they express Uncoupling Protein 1 (UCP1), which embeds in the inner mitochondrial membrane and produces heat by uncoupling oxidative metabolism from ATP production. The energy expending properties of brown adipocytes coupled with the observation that human BAT amount inversely correlates with body fat mass (Cypess et al., 2009; van Marken Lichtenbelt et al., 2009) is garnering interest in developing strategies to increase brown adipocyte number and/or activity to treat obesity (Harms and Seale, 2013; Nedergaard and Cannon, 2010; Tseng et al., 2010). However, the mechanisms—and in particular the signaling circuitry—by which BAT regulates its energy supply and usage are poorly understood (Townsend and Tseng, 2014). With the obesity pandemic seemingly out of control, and with a desperate need for novel therapeutics, the importance of elucidating mechanisms controlling adipocyte growth and function cannot be overstated.

Studying the in vivo mechanisms that control adipose tissue growth has been challenging because adipocyte origins are not well understood and consequently there are few tools available that are useful for genetically targeting adipocyte precursors in vivo (e.g. by Cre-Lox). Mesenchymal precursors cells expressing *Myf5* give rise to myocytes, brown adipocytes, and a subset of white adipocytes (Sanchez-Gurmaches and Guertin, 2014b; Sanchez-Gurmaches et al., 2012; Seale et al., 2008) and several recent studies have

successfully used the *Myf5-cre* knock-in allele (Tallquist et al., 2000) to study brown adipose tissue development (Harms et al., 2014; Martinez-Lopez et al., 2013; Ohno et al., 2013; Sanchez-Gurmaches et al., 2012; Schulz et al., 2013). Thus, the multi-fate potential of *Myf5* precursors provides an opportunity to use genetics to distinguish between signaling mechanisms that are required in vivo for the growth of myocytes versus adipocytes.

The mechanistic target of rapamycin (mTOR) kinase is a master-regulator of growth that functions in at least two distinct complexes called mTORC1 (defined by the Raptor subunit) and mTORC2 (defined by the Rictor subunit) (Laplante and Sabatini, 2012). While much is known about the inputs, outputs, and regulatory features of mTORC1, mTORC2 regulation and function remains more enigmatic (Ben-Sahra et al., 2013; Laplante and Sabatini, 2012; Robitaille et al., 2013). The best-described biochemical function of mTORC2 is to phosphorylate the hydrophobic motif (HM) of AKT (S473 in AKT1) and the related SGK (S422 in SGK1) kinases (Garcia-Martinez and Alessi, 2008; Sarbassov et al., 2005). AKT has many effectors including GSK3β, FoxO1/3, and mTORC1 (through TSC2 and PRAS40) and most models indicate mTORC2 is an essential upstream regulator of pan-AKT activity (Laplante and Sabatini, 2012). However, the extent to which this is the case in vivo remains unclear because *Rictor* deficient mouse embryo fibroblasts, which lack mTORC2, have seemingly normal GSK3β phosphorylation, mTORC1 activity, and only partially decreased FoxO1/3 phosphorylation (Guertin et al., 2006; Jacinto et al., 2006; Shiota et al., 2006).

Mice lacking *Rictor* die around E10.5 (Guertin et al., 2006; Jacinto et al., 2006; Shiota et al., 2006); therefore, mTORC2 function in vivo is mostly being investigated using floxed *Rictor* alleles. In adipose tissue, two studies using *aP2-cre* to delete *Rictor* reported no effect on individual adipocyte size or overall adipose tissue mass (Cybulski et al., 2009; Kumar et al., 2010). One of the studies finds *aP2-cre;Rictor*$^{fl/fl}$ mice eventually develop mild glucose intolerance and ectopic lipid deposition although a mechanism was not elucidated (Kumar et al., 2010). Notably however, the utility of *aP2-cre* as a tool to target adipocytes has recently been questioned (Lee et al., 2013; Mullican et al., 2013; Wang et al., 2013);

therefore, the exact function of mTORC2 in adipose tissue remains unclear. Deleting *Rictor* in skeletal muscle with *Hsa-cre* or *Mck-cre* also has no effect on muscle fiber size or overall muscle mass and only minor effects on insulin-mediated glucose metabolism (Bentzinger et al., 2008; Kumar et al., 2008). The relatively mild phenotypes associated with conditional ablation of *Rictor* in adipose tissue and muscle are somewhat surprising considering the importance of AKT and its downstream effectors in metabolism; however, in both cases (adipose tissue and muscle) the Cre drivers mentioned above reportedly target mature cells and thus the in vivo role of mTORC2 in adipose tissue and muscle precursors is unknown.

Here, we take advantage of the fact that *Myf5-cre* expresses in precursors of muscle and brown adipocytes to investigate the role of Rictor (i.e. mTORC2) and for comparison Raptor (i.e. mTORC1) in muscle and BAT growth. We report that *Raptor* is essential in the *Myf5* lineage for myogenesis, establishing BAT precursors, and viability. In contrast, *Rictor* is dispensable for myogenesis and viability, but essential for normal BAT growth. Moreover, Rictor-deficient BAT is more metabolically active, having elevated mitochondrial activity, decreased lipogenesis gene expression, and reduced lipid storage. Importantly, deleting *Rictor* in the *Myf5*-lineage also augments diet-induced thermogenesis, which protects mice from an obesogenic diet at thermoneutrality. We also find that *Myf5*-lineage white adipocytes require Rictor for normal growth in vivo suggesting a broader role for mTORC2 in adipose tissue growth. Finally, we show that Rictor is also required in vitro for brown adipocyte differentiation but not for pan-AKT activity, and that this differentiation defect is rescued with BMP7. Collectively, our results provide new insight into the in vivo and in vitro regulation of brown adipocytes and implicate Rictor/mTORC2 as a critical signaling node that regulates the balance between oxidative and lipogenic metabolic states.

Results

Rictor is dispensable in the *Myf5* lineage during embryogenesis

Precursors expressing *Myf5* give rise to brown adipocytes, a subset of white adipocytes, and skeletal muscles (Sanchez-Gurmaches and Guertin, 2014a; Sanchez-Gurmaches et al., 2012; Seale et al., 2008). We took advantage of this to investigate the role of mTORC1 versus mTORC2 in vivo in fat versus muscle development by generating *Myf5-cre;Raptor*$^{fl/fl}$ (*Raptor*^{Myf5cKO}) and *Myf5-cre;Rictor*$^{fl/fl}$ (*Rictor*^{Myf5cKO}) conditional knockout mice. The *Rictor*^{Myf5cKO} mice are born at the expected Mendelian ratio and show no obvious motor or behavioral defects [not shown]. In contrast, *Raptor*^{Myf5cKO} mice die perinatally. E16.5 *Raptor*^{Myf5cKO} embryos are smaller due to a muscle development defect that is not apparent in control or *Rictor*^{Myf5cKO} embryos [Figure S1A-D]. For example, transverse sections through the head and neck of *Raptor*^{Myf5cKO} embryos reveal an underdeveloped tongue and the absence of the masseter, sternohyoid, hyglossus, supraspinatus, prevertebral, and trapezius muscles, the later deficiency resulting in hind neck body wall fragility during specimen preparation [Figure S1A-D]. Thus, *Raptor* is essential in the *Myf5* lineage for viability and muscle development while *Rictor* is dispensable for both.

To confirm that *Rictor* is dispensable for myogenesis, we purified satellite cells (which express *Myf5*) from *Rictor*^{Myf5cKO} skeletal muscles, confirmed they are deleted for *Rictor* [Figure S1E], and show they differentiate ex vivo into myosin heavy chain-positive multinucleate myofibers [Figure S1F-G]. Moreover, deleting *Raptor* in satellite cells in vivo with Pax7-CreER completely blocks skeletal muscle repair, while deleting *Rictor* by the same approach does not prevent muscle regeneration following acute injury [Figure S1H-I]. Thus, Rictor is also dispensable for satellite cell differentiation ex vivo and for adult myogenesis induced by injury.

White adipose tissues develop postpartum in mice, but early brown adipocyte precursor cells (bAPCs) are easily detectable in E16.5 embryos by Hematoxylin and Eosin

(H&E) stain. Qualitatively similar pools of cervical, interscapular, and subscapular bAPCs are clearly detectable in control and *Rictor*^{Myf5cKO} E16.5 embryos [Figure S1A & S1D]. In contrast, interscapular and subscapular bAPCs are absent in E16.5 *raptor*^{Myf5cKO} embryos [Figure S1A & S1D]. Notably, a diminished pool of cervical bAPCs is detectable in the *Raptor*^{Myf5cKO} embryos, which is consistent with our lineage tracing data showing that only about half of the cervical brown adipocytes arise from *Myf5-cre* expressing precursors [Figure 1SD](Sanchez-Gurmaches and Guertin, 2014b). Thus, Raptor but not Rictor is also essential in the *Myf5*-lineage for establishing bAPCs during embryogenesis.

Brown and white adipose tissue growth requires Rictor

Although Rictor^{Myf5cKO} mice show no obvious embryonic phenotypes, they tend to weigh less (not significantly) than controls at postnatal day 1 (P1) [Figure S1J], which reaches significance from 6-15 weeks of life [Figure 1A]. Individual tissue analysis indicates that the weight difference results from decreased adipose tissue mass. For example, the interscapular BAT (iBAT) in P1 Rictor^{Myf5cKO} neonates weighs about 30% less than normal [Figure S1K] and during the first weeks of life the mutant BAT grows but to a much smaller size, resulting in mutant iBAT and subscapular BAT (sBAT) depots at 6-weeks weighing about 50% less than controls and being darker in color [Figure 1B]. Adipocytes in the retroperitoneal and anterior subcutaneous WAT depots (rWAT, asWAT) are also derived largely from *Myf5-cre* expressing precursors (Sanchez-Gurmaches et al., 2012) and both of these depots also decrease in mass by approximately 50% in the *Rictor*^{Myf5cKO} mice [Figure 1C]. In contrast, the posterior subcutaneous and peri-gonadal WAT depots (psWAT, pgWAT), which are composed of *Myf5*-negative lineage adipocytes, do not differ in weight [Figure 1C]. Skeletal muscles (e.g. triceps, quadriceps, and gastrocnemius) and all other lean tissues examined except the kidneys (which are slightly larger) are normal size in the knockout [Figure 1D]. Western analysis for Rictor protein confirms *Rictor* deletion and reduced AKT-S473 phosphorylation in iBAT and muscle and to a lesser extent in rWAT and asWAT, but not in psWAT, pgWAT or liver [Figure 1E].

From 6 weeks to 6 months, the mutant iBAT and sBAT shows no additional growth increase while asWAT and rWAT grow to about half (asWAT) or one third (rWAT) the size of their anatomically matched control tissues [Figure 1F]. In contrast, *Rictor*^{Myf5cKO} psWAT, pgWAT, muscles, and liver grow to their normal size in the same time frame [Figure 1F]. Thus, *Rictor*^{Myf5cKO} mice can grow small BAT tissues in the first weeks of life; however, as *Rictor*^{Myf5cKO} mice age the iBAT and sBAT maintain their weight while asWAT and rWAT grow at a reduced rate. Collectively, these results indicate Rictor is essential in the *Myf5* lineage for adipose tissue growth but not for skeletal muscle growth.

Brown adipocytes lacking Rictor are smaller

To better define the BAT growth defect we histologically examined iBAT in control and *Rictor*^{Myf5cKO} mice. At E18.5 there is no qualitative difference between control and *Rictor*^{Myf5cKO} bAPCs pools [Figure 2A]. In P1 neonates however, lipids begin accumulating in control BAT but not in the *Rictor*^{Myf5cKO} BAT [Figure 2A]. From P1 to 6 months lipid droplets grow in size in control BAT but remain small in the *Rictor*^{Myf5cKO} BAT [Figure 2A] resulting in smaller cells measured by the increase in nuclei per mm^2 [Figure S2A]. Total genomic DNA content (an indirect measure of cell number) is also lower in the *Rictor*^{Myf5cKO} BAT indicating additional tissue hypoplasia [Figure S2B]. In contrast, *Rictor*^{Myf5cKO} skeletal muscle fibers appear histologically identical to control fibers [Figure S2C] consistent with Rictor being dispensable for myocyte growth.

Myf5-lineage white adipocytes lacking Rictor are also small and multilocular

Compared to controls, many of the adipocytes in the *Rictor*^{Myf5cKO} rWAT and asWAT are also smaller and multilocular [Figure 2B] but the pattern is heterogeneous in that several large unilocular white adipocytes are also detectable. The appearance of psWAT and pgWAT adipocytes is unchanged in the knockout [Figure S2C]. We recently discovered that the adipocyte precursor pools in rWAT and asWAT are a mix of *Myf5-cre* lineage positive and negative precursors (Sanchez-Gurmaches et al., 2012). Therefore, we reasoned that the size heterogeneity in *Rictor*^{Myf5cKO} rWAT and asWAT could reflect a

mosaic of *Myf5*-lineage negative (i.e. undeleted) and *Myf5*-lineage positive (i.e. *Rictor* knockout) cells. To test this we incorporated the *Rosa26-mTmG* reporter (Muzumdar et al., 2007) into control and *Rictor*^{Myf5cKO} mice to irreversibly label Cre-expressing cells and their lineages with membrane-targeted eGFP (mGFP); all other (Cre^{neg}) cells and their descendants are labeled with membrane targeted tdTomato fluorescent protein (mTFP). The result is unequivocal; only the small adipocytes are mGFP^{+} in *Rictor*^{Myf5cKO} rWAT and asWAT while all the large unilocular adipocytes are mTFP^{+} [Figure 2C]. As expected, in both the control and *Rictor*^{Myf5cKO} mice the iBAT adipocytes are mGFP^{+} and the psWAT and pgWAT adipocytes are mTFP^{+} [Figure S2D]. We examined UCP1 expression by immunohistochemistry in the asWAT and rWAT and detect a slight increase in UCP1 staining in the *Rictor*^{Myf5cKO} adipocytes suggesting the cells might have brown-adipocyte like characteristics [Figure S2E](not shown). Nevertheless, these data confirm that the heterogeneous small cell phenotype in the *Myf5*-lineage white adipocytes is the result of cell-autonomous *Rictor* deletion.

Lipogenesis is decreased in Rictor-deficient BAT

We hypothesized that the paucity of lipid and marked color difference between control and *Rictor*^{Myf5cKO} BAT indicates a metabolic shift to a more oxidative state. To test this we first examined AKT signaling in BAT, which positively regulates lipogenesis. In vivo PDK1-mediated AKT-T308 phosphorylation is intact in both fasted/re-fed and insulin-stimulated *Rictor*^{Myf5cKO} BAT despite ablation of phospho-AKT S473 and phospho-AKT T450 (which is also mTORC2 dependent) [Figure 3A & S3A], consistent with the ability of T-loop (T308) and hydrophobic motif (S473) phosphorylation to be regulated independently (Pearce et al., 2010). Surprisingly, phosphorylation of the classic AKT substrates FoxO1/3, GSK3β, TSC2, PRAS40, and AS160 is normal in *Rictor*^{Myf5cKO} BAT [Figure 3A] indicating that Rictor is not essential in BAT for pan-AKT signaling. Rictor loss in BAT also does not affect phosphorylation of the SGK substrate NDRG1 [Figure 3A] indicating mTORC2 is also not essential in BAT for SGK signaling to NDRG1 or that a compensatory pathway exists.

Next we examined whether deleting *Rictor* in the *Myf5*-lineage affects expression of BAT differentiation markers. In P1 neonates, *Prdm16*, *C/ebpα,* and C*/ebpβ* expression do not significantly differ between controls and knockouts, while *Pparγ* and *Ucp1* levels slightly decrease [Figure 3B] indicating a possible delay in BAT maturation in the knockouts. However, by 6 weeks *Pparγ*, *Prdm16,* and *C/ebpα* all express at control levels while *C/ebpβ*, *Ucp1*, and *Dio2* express at significantly higher than control levels [Figure 3B]. The mature adipocyte markers *Cidea* and *aP2* are unchanged between control and knockout both at P1 and 6 weeks [Figure 3B]. Consistent with the gene expression data, PPARγ, UCP1, and insulin receptor beta (IRβ) proteins also express at near control levels in *Rictor*^{Myf5cKO} BAT [Figure 3A]. Thus, while brown adipocyte maturation may be slightly delayed in late embryonic or early neonatal development, terminal differentiation per se (i.e. PPARγ, UCP1, and IRβ induction) occurs in *Rictor*^{Myf5cKO} brown adipocytes and if anything, the *Rictor*^{Myf5cKO} BAT exhibits a stronger "brown" signature.

Next we examined lipogenesis genes. In P1 *Rictor*^{Myf5cKO} BAT, acetyl-coA carboxylase (*Acc*), fatty acid synthase (*Fasn)*, and fatty acid elongase 6 (*Elovl6*) decrease expression by (40%), (40%), and (25%) respectively [Figure 3C]. By 6 weeks, expression of ATP citrate lyase (*Acly)* in addition to *Acc, Fasn,* and *Elovl6* is reduced by 90%, 75%, 80%, and 40% respectively [Figure 3C], which we confirmed by Western blot for ACLY and ACC [Figure 3A]. In addition, stearoyl-CoA desaturase (*Scd1*) decreases expression by 45% in 6 week *Rictor*^{Myf5cKO} BAT [Figure 3C]. The SREBP1c and ChREBP transcription factors regulate lipogenesis gene expression (Czech et al., 2013; Filhoulaud et al., 2013). In both P1 and 6-week *Rictor*^{Myf5cKO} BAT, the mRNA expression of SREBP1c (*Srebf1c*), which is induced by insulin, and ChREBP (α and β isoforms), which is induced by glucose, is similar [Figure 3D]. However, there is a marked decrease in the amount nuclear SREBP1c (nSREBP1c), the transcriptionally active SREBP1c cleavage product, in the Rictor-deficient BAT [Figure 3A] consistent with the decrease in lipogenic gene expression. The levels of *insig1,* another nSREBP1c target gene and negative regulator of SREBP1c processing, also decreases [Figure 3C]. The mRNA expression of SREBP2 (which regulates cholesterol biosynthesis) slightly decreases in *Rictor*^{Myf5cKO} BAT at 6 weeks, but the SREBP2 target

genes HMG-CoA synthase (*Hmg-cs)* and HMG-CoA reductase (*Hmg-cr*) express at similar levels in control and knockout BAT [Figure 3D] and nuclear SREBP2 protein (nSREBP2) accumulates possibly to even higher levels in the knockout BAT [Figure 3A]. The post-translational regulation of ChREBP is poorly understood and therefore we could not determine if ChREBP protein function is normal. We also find no difference in AMPK phosphorylation (which is a negative regulator of lipogenesis) between control and *Rictor*^{Myf5cKO} BAT [Figure 3A] or in hormone sensitive lipase (HSL) phosphorylation [Figure S3A]. Together, these results indicate that despite having seemingly normal AKT signaling, de novo lipogenesis is dramatically reduced in *Rictor*^{Myf5cKO} BAT.

Mitochondrial activity is elevated in Rictor-deficient BAT

To further examine the metabolic state of *Rictor*^{Myf5cKO} BAT we next examined mitochondrial activity. In P1 neonate *Rictor*^{Myf5cKO} BAT, *Pgc1a* expresses normally, while expression of mitochondrial transcription factor A (*Tfam)*, which regulates mtDNA replication, and carnitine palmitoyltransferase 1B *(Cpt1b)*, which encodes the rate-limiting enzyme in beta-oxidation, slightly decreases [Figure 4A]. Thus, increased mitochondrial activity does not appear to accompany the lipogenesis defect in P1 *Rictor*^{Myf5cKO} neonates. In contrast, *Pgc1a*, *Tfam*, and *Cpt1b* in addition to *Ucp1* express at significantly higher levels in the BAT of 6-week old *Rictor*^{Myf5cKO} mice [Figure 4A & 3B] suggesting overall BAT mitochondrial activity progressively increases in the *Rictor*^{Myf5cKO} mice as they age.

To explore this in more detail, we used qRT-PCR arrays to broadly measure mitochondrial gene expression in the 6-week old BAT. Using arrays for functional genes involved in mitochondrial molecular transport and biogenesis (including *Ucp1* and *Cpt1b*), we detect significant increases in several genes in addition to *Ucp1* and *Cpt1b* that indicate increased mitochondrial activity [Figure 4B]. Furthermore, the mitochondrial citrate and malate transporters *Slc25a1* and *Slc25a10* respectively—both of which function in fatty acid biosynthesis, the former also being an SREBP1c target gene (Infantino et al., 2007; Mizuarai et al., 2005)—significantly decrease expression in the mutant BAT. Using mitochondrial energy metabolism gene arrays, we found 58 additional genes involved in

respiration to also be significantly elevated in *Rictor*^{Myf5cKO} BAT relative to controls [Figure S4A] suggesting an increase in overall mitochondrial mass, which we confirmed by immunofluorescence staining with CoxIV [Figure 4C]. Transmission electron microscopy (TEM) further reveals individual mitochondria in the mutant BAT are morphologically larger and have more disorganized cristae [Figure 4D]. To directly confirm that mitochondrial activity is elevated, we measured the oxygen consumption rate (OCR) of control and *Rictor*^{Myf5cKO} BAT in a Seahorse Flux Analyzer and determined that both basal and pyruvate-stimulated OCR are elevated by around 18% in *Rictor*^{Myf5cKO} BAT [Figure 4E]. We did not detect a significant increase in overall oxygen consumption when *Rictor*^{Myf5cKO} mice were placed in metabolic cages at 22°C except when normalized for body weight [Figure S4B]. Notably however, mice are under thermal stress at this temperature, which can mask effects on BAT activity (Feldmann et al., 2009).

Interestingly, we also detect an approximate 2-fold increase in basal glucose uptake in *Rictor*^{Myf5cKO} BAT measured by ^{18}FDG-PET CT scanning [Figure S4C] and a significant increase in lipoprotein lipase (*Lpl*) expression [Figure 3C] suggesting that *Rictor*^{Myf5cKO} BAT may consume more nutrients than age matched control BAT. Small metabolite profiling reveals that *Rictor*^{Myf5cKO} BAT also has elevated levels of inosine monophosphate (IMP) [Figure S4D], a deamination product of adenosine monophosphate (AMP), the accumulation of which suggests increased uncoupling (Balcke et al., 2011). In an acute cold challenge Rictor-deficient BAT also induces *Ucp1* expression significantly more than control BAT and the mutants have no difficulty maintaining body temperature, although notably body temperature regulation in an acute cold challenge is largely a function of muscle [Figure 4F]. Finally, we see no compensatory "browning" in the psWAT as would be expected if *Rictor*^{Myf5cKO} BAT were dysfunctional [Figure S2C-D](Schulz et al., 2013). These results are consistent with Rictor loss in BAT shifting metabolism to a more oxidative and less lipogenic state.

Brown preadipocytes require Rictor to differentiate in vitro

To examine if the brown adipocyte differentiation program also requires Rictor in vitro, we generated brown adipocyte precursor cells (bAPCs) harboring an inducible knockout system (i.e. *Rictor*^{iKO}) in which *Rictor* deletion is triggered by 4-hydroxytamoxifen (4-OHT) [Figure S5A]. The advantage of this approach is that acute *Rictor* loss can be compared to isogenic controls. Inducibly deleting *Rictor* rapidly and robustly depletes Rictor protein and AKT-S473 phosphorylation, and consistent with our in vivo data, leaves AKT-T308 phosphorylation intact [Figure S5B]. Also consistent with the in vivo results, both basal and insulin-stimulated phosphorylation of FoxO1/3, GSK3β, TSC2, and PRAS40 are normal in *Rictor*^{iKO} bAPCs [Figure 5A]. S6K1 phosphorylation is also unaffected [Figure 5A]. Contrary to the in vivo results, acute *Rictor* loss in vitro decreases phosphorylation of the SGK target NDRG1 [Figure 5A]. This indicates Rictor is required in cultured bAPCs for SGK activity to NDRG1 but not for pan-AKT or mTORC1 activity.

To our surprise, *Rictor*^{iKO} bAPCs are completely incapable of synthesizing lipid droplets in vitro when induced to differentiate [Figure 5B]. This is surprising because *Rictor*^{iKO} cells maintain normal levels of AKT-T308, GSK3β-S9, and S6K1-T389 phosphorylation (i.e. PDK1, AKT, and mTORC1 activity respectively) throughout the differentiation protocol [Figure 5C]. The differentiation block occurs early as *Rictor*^{iKO} bAPCs fail to induce *C/ebpα*, *Pparγ*, *Prdm16, Pgc1α*, *Srebf1c*, *Ucp1,* and *Glut4* [Figure 5D & S5C]. The expression of *C/ebpδ* and *C/ebpβ* on the other hand induces normally and slightly higher in the *Rictor*^{iKO} bAPCs respectively at differentiation day 6 [Figure 5D]. Consistent with the gene expression data, PPARγ, IRβ, UCP1, nSREBP1c, ACC, and ACLY levels fail to increase during differentiation in *Rictor*^{iKO} bAPCs [Figure 5E]. Notably, 4-OHT or CreER activation alone (i.e. in the absence of *Rictor* floxed alleles) has no effect on differentiation [not shown]. Moreover, bAPCs prepared from P1 *Rictor*^{Myf5cKO} neonates also fail to differentiate in vitro indicating that the ex vivo differentiation block is not unique to using the inducible knockout-system [Figure S5D]. Importantly, expressing recombinant PPARγ in *Rictor*^{iKO} bAPCs rescues IRβ, UCP1 and nSREBP1c expression [Figure 5F] and lipid droplet production [Figure 5G] in the absence of Rictor indicating that Rictor promotes bAPC differentiation at least in part by facilitating PPARγ induction.

Insulin receptor substrate 1 (*Irs1*) and *Irs3* knockout bAPCs also fail to induce PPARγ ex vivo (Fasshauer et al., 2001). It was later shown that *Irs1/3* KO bAPCs are unable to differentiate because they express high levels of *Pref-1*, *Wnt10a*, and *Necdin*, which encode adipogenesis inhibitors (Tseng et al., 2005). In contrast, *Rictor*-deficient bAPCs express normal levels of *Pref-1*, *Wnt10a*, and *Necdin* in culture, and during differentiation *Necdin* and *Pref-1* increase but only late in the differentiation protocol [Figure S5C]. Thus, the mechanism by which deleting *Rictor* inhibits brown adipocyte differentiation differs from that of deleting *Irs1/3*.

AKT1 functions downstream of Rictor in brown adipocyte differentiation

To further explore the mechanism by which Rictor regulates brown adipocyte differentiation, we next asked whether an AKT or SGK pathway is required downstream of Rictor for differentiation in vitro. To this end, we generated *Rictor*^{iKO} bAPCs that express HA-SGK1, HA-AKT1, HA-AKT2, or their phosphomimetic counterparts HA-SGK-S422D, HA-AKT1-S473D, HA-AKT2-S474D in which a phosphomimetic residue was placed at the mTORC2 hydrophobic motif site, and asked whether any of these constructs rescue differentiation. Only HA-AKT1-S473D efficiently rescues lipid biosynthesis [Figure 6A]. HA-AKT1-S473D-expressing *Rictor*^{iKO} bAPCs also induce PPARγ to control levels, and consequently, IRβ, UCP1, nSREBP1c, ACLY, and ACC expression are all restored [Figure 6B]. We confirmed that all of the recombinant proteins are functional [Figure S6A]. Thus, Rictor promotes differentiation as part of mTORC2 and through an AKT pathway, not an SGK pathway.

Our rescue experiments point to AKT1 as the specific isoform driving bAPC differentiation in vitro. Consistent with this notion, AKT1 is more highly expressed in undifferentiated precursors and decreases expression during differentiation while AKT2 expresses at lower levels in undifferentiated precursors and induces late during differentiation [Figure S6B]. To further examine the role of AKT1 and AKT2 in bAPC differentiation, we created *Myf5-cre;Akt1*^{floxed} and *Myf5-cre;Akt2*^{floxed} mice and from them

generated bAPC lines that specifically lack either *Akt1* or *Akt2* and determined their vitro differentiation capacity. Consistent with AKT1 but not AKT2 being more essential for differentiation, *Akt1*-deficient bAPCs cannot efficiently synthesize lipid droplets [Figure S6C] or up-regulate PPARγ, IRβ, or UCP1 when induced to differentiate [Figure S6D]. In contrast, *Akt2*-deficient bAPCs induce PPARγ, IRβ, and UCP1 to control levels [Figure S6C] indicating that AKT1 is indeed the isoform required downstream of Rictor/mTORC2 for brown adipocyte differentiation.

BMP7 rescues brown adipocyte differentiation in the absence of Rictor

Our in vitro studies uncovered a paradoxical relationship between our in vivo and in vitro models; in vitro *Rictor*^{iKO} bAPCs cannot differentiate (i.e. induce PPARγ and UCP1), but in vivo Rictor-deficient BAT clearly develops and is positive for both PPARγ and UCP1. We had first hypothesized that in vitro bAPCs might require SGK activity to differentiate because SGK activity is decreased in vitro but not in vivo in the absence of Rictor; however, our rescue experiments with recombinant phosphomimetics argue against this. An alternative hypothesis is that in vivo, in the natural environment, there are developmental signals present that are missing from the artificial in vitro differentiation assay. The signals that drive brown adipocyte differentiation in vivo are poorly understood. One proposed inducer of brown adipocyte differentiation is the transforming growth factor-β superfamily member BMP7 (Schulz and Tseng, 2013; Tseng et al., 2008). When given to control or *Rictor*^{iKO} bAPCs, BMP7 does not induce AKT phosphorylation [Figure 6C]. However, when supplemented into the differentiation cocktail BMP7 restores to *Rictor*^{iKO} bAPCs their ability to synthesize lipid droplets [Figure 6D] and express PPARγ, IRβ, UCP1 and to a lesser extent nSREBP1c, ACLY, and ACC [Figure 6E]. These results are consistent with the in vitro differentiation assay lacking key signaling molecules present in vivo and suggest that BMP7 signaling converges with Rictor/mTORC2-AKT1 signaling on a downstream effector during brown adipocyte differentiation.

Interestingly, in our in vitro differentiation assays with *Akt1* and *Akt2* deficient bAPCs, we noticed that while the *Akt2*-deficient cells differentiate, they fail to induce nSREBP1C and consistently ACLY and ACC express at low levels [Figure S6D]. This suggests that while AKT2 is not essential for brown adipocyte differentiation, it is important downstream of Rictor/mTORC2 for regulating lipid metabolism in mature brown adipocytes. Consistent with this idea, when we immunoprecipitate AKT1 or AKT2 from undifferentiated control and *Rictor*^{iKO} bAPCs, all of the detectable AKT phosphorylation is on AKT1 while in vivo the bulk of AKT phosphorylation appears to shift to AKT2 [Figure S6E-F]. Thus, while the inability of *Rictor*^{iKO} bAPCs to differentiate in culture in the absence of BMP7 reflects an AKT1 pathway deficiency, the in vivo metabolic phenotype appears to reflect an AKT2 pathway deficiency.

Rictor^{Myf5cKO} mice are less susceptible to obesity and metabolic disease at thermoneutrality

The higher metabolic activity of Rictor-deficient BAT led us to wonder whether *Rictor*^{Myf5cKO} mice are resistant to obesity. Chronic consumption of high fat diet (HFD) triggers a phenomenon in mice called diet-induced thermogenesis, which requires UCP1, and counteracts obesity (Cannon and Nedergaard, 2010; Feldmann et al., 2009). Because BAT activity is masked by chronic thermal stress at 22°C (the temperature of our mouse facility), we conducted the following studies at thermoneutrality (30°C for mice), which exempts mice from this thermal stress (Feldmann et al., 2009). When living at 30°C and eating a normal chow diet (chow), control and *Rictor*^{Myf5cKO} mice gain roughly the same amount of weight [Figure 7A] and consume the same amount of total energy [Figure 7B] over a 12-week span. In contrast, when living at 30°C and eating a HFD (45% calories from fat), control mice gain on average 14.67±1.054 grams of weight while *Rictor*^{Myf5cKO} mice only gain 10.570±1.178 grams [Figure 7A] despite both groups again consuming the same amount of total energy [Figure 7B]. This translates into the control cohort gaining 64% more weight when eating HFD versus chow than the *Rictor*^{Myf5cKO} mice and suggests the *Rictor*^{Myf5cKO} mice living at thermoneutrality and eating a HFD are less metabolically efficient than controls, which is indeed the case [Figure 7C].

The resistance to weight gain in the HFD-fed *Rictor*^{Myf5cKO} cohort is partly due to reduced growth of adipose tissue. For example, the pgWAT (the largest white fat depot) gains significantly less mass in the HFD-fed *Rictor*^{Myf5cKO} cohort than in HFD-fed controls [Figure 7D]. The liver and heart also grow larger in the control cohort eating HFD compared to the control cohort eating chow, while the liver and heart grow to the same mass in the *Rictor*^{Myf5cKO} cohorts regardless of the diet [Figure 7D & S7A]. Diet also has no effect on the growth of other lean tissues including skeletal muscles (quadriceps and gastrocnemius), kidney, or pancreas in either the controls or *Rictor*^{Myf5cKO} cohorts [Figure 7D & S7A]. That pgWAT grows less in HFD-fed *Rictor*^{Myf5cKO} mice compared to chow-fed controls indicates systemic protection against obesity is occurring because *Myf5*-Cre does not target pgWAT [Figure 1F & S2C]. The reduction in pgWAT mass is due at least in part to smaller adipocyte size [Figure 7E]; the livers of *Rictor*^{Myf5cKO} mice are also resistant to developing hepatic steatosis [Figure 7E]; and the HFD-fed *Rictor*^{Myf5cKO} mice perform better in a glucose tolerance test [Figure S7B], all consistent with systemic protection from obesity.

In the chow-fed cohorts living without thermal stress, histology reveals that control BAT adopts a more "white adipocyte-like" appearance—that is the lipid droplets appear larger and unilocular [Figure 7E]. In contrast, the BAT in chow-fed *Rictor*^{Myf5cKO} mice resists the whitening effects of living at thermoneutrality and maintains more of a "brown-adipocyte-like" appearance [Figure 7E]. This resistance to whitening is reflected in the gene expression signature using recently identified BAT and WAT identity genes (Harms et al., 2014; Walden et al., 2011); for example, when normalized to BAT gene expression at 22°C, the shift to thermoneutrality decreases the expression of BAT-selective genes (*Prdm16, Sgk2, cideb, cyp2b10*) and increases the expression of WAT-selective genes (*Dpt1, Retn, Trim14, Nnmt*) to a greater extent in control BAT than in *Rictor*^{Myf5cKO} BAT, which maintains a more BAT-like identity. [Figure S7C]. Thus, the BAT of *Rictor*^{Myf5cKO} mice consuming chow is resistant to the whitening effects of removing thermal stress.

In the HFD-fed cohorts living without thermal stress, histology reveals a large number of multi-locular adipocytes in the control BAT [Figure 7F] that are not apparent in the chow-fed controls [Figure 7E] suggesting diet-induced thermogenesis. This is also reflected in the gene expression data as *Prdm16* levels increase in control BAT in HFD-fed mice compared to chow-fed [Figure 7G], while the WAT-specific genes *Retn, Trim14,* and *Nnmt* decrease [Figure 7G]. The histology also reveals that *Rictor*^{Myf5cKO} BAT is even more "brown-like" in the HFD-fed cohort exhibiting a uniform abundance of small lipid droplets [Figure 7F] and a stronger BAT-identity gene signature (i.e. elevated *Prdm16, Sgk2, Cideb, Cyp2b10*; decreased *Dpt1, Retn, Trim14, Nnmt*)[Figure 7G]. Consistent with the Rictor-deficient BAT being more stimulated by HFD, BAT functional genes (*Ucp1*, *Pgc1α*, *Cpt1β*, *Dio2*) induce to a greater extent in the BAT of HFD-fed *Rictor*^{Myf5cKO} mice [Figure 7H], which maintain relatively low levels of *Acly*, *Acc*, and *Fasn* expression [Figure S7D]. Consistently, UCP1 protein level is higher in the BAT of *Rictor*^{Myf5cKO} mice eating HFD [Figure 7I]. Interestingly, after 20 weeks of eating a HFD, the control BAT eventually reverts back to a more "white-adipocyte-like" histology; however, BAT character is preserved in the *Rictor*^{Myf5cKO} mice [Figure S7E]. Collectively, these results suggest that inhibiting mTORC2 in BAT increases diet-induced thermogenesis and consequently, *Rictor*^{Myf5cKO} mice living without thermal stress and consuming an obesogenic diet are less susceptible to developing obesity and metabolic disease.

DISCUSSION

While transcriptional regulation of BAT development and function has been extensively described (Cristancho and Lazar, 2011; Kajimura et al., 2010), much less is known about the signaling mechanisms that regulate BAT. The control of brown fat fuel utilization is also incompletely understood (Townsend and Tseng, 2014). Previous studies reported that conditionally deleting *Rictor* in white and brown adipose tissue or skeletal muscle has no affect on WAT or BAT mass or individual adipocyte or myocyte size (Bentzinger et al., 2008; Cybulski et al., 2009; Kumar et al., 2008; Kumar et al., 2010). However, these studies used Cre drivers that reportedly delete *Rictor* in mature cells, which led us to hypothesize that Rictor/mTORC2 may be more important in vivo for brown/white adipose tissue and/or muscle development. By conditionally deleting *Rictor* in *Myf5* precursors, which give rise to brown adipocytes, a subset of white adipocytes, and myocytes (Sanchez-Gurmaches and Guertin, 2014b; Sanchez-Gurmaches et al., 2012; Seale et al., 2008) we discovered that Rictor is not essential in vivo for muscle development or regeneration. In contrast, *Myf5*-lineage brown and white adipocytes lacking Rictor are reduced in size. Furthermore, Rictor-deficient BAT undergoes a metabolic shift to a more oxidative and less lipogenic metabolic, despite having normal pan-AKT signaling. Importantly, at thermoneutrality this protects mice against an obesogenic diet. These findings implicate Rictor/mTORC2 as an essential signaling node in BAT that regulates the balance between fatty acid oxidation and storage. Considering that active BAT is now recognized to exist in adult humans, our findings could have important implications for understanding the signaling mechanisms that regulate fuel usage and metabolic activity in human BAT.

We also report that in vitro brown adipocyte differentiation requires Rictor/mTORC2. Mechanistically, Rictor/mTORC2 promotes *Pparγ* induction through AKT1 independently of pan-AKT signaling and mTORC1 activity. In vivo however, brown adipocytes differentiate in *Rictor*^{Myf5cKO} mice despite lacking Rictor expression. We hypothesize that this paradox indicates that the artificial in vitro culture conditions lack an

555 important signal present in vivo that can overcome this deficiency. Supporting this notion,
556 supplementing the differentiation assay with BMP7, a proposed in vivo inducer of brown
557 adipocyte differentiation and thermogenesis (Schulz and Tseng, 2013; Tseng et al., 2008),
558 rescues differentiation in the absence of Rictor. Notably, we do in fact detect low *pparγ*
559 expression in *Rictor*^{Myf5cKO} P1 BAT, which may reflect the role of Rictor/mTORC2 in early
560 brown adipocyte differentiation and explain the mutant BAT hypoplasia. Exactly how
561 Rictor/mTORC2 and BMP7 signaling might converge on PPARγ is not yet clear. We also
562 show that during brown adipocyte differentiation, the major AKT isoform switches from
563 AKT1 to AKT2; thus, while Rictor/mTORC2 may regulate differentiation through an AKT1
564 pathway that can be bypassed in vivo, its role in BAT metabolism is likely mediated
565 through an AKT2 pathway that cannot be compensated for. Consistent with this idea,
566 whole body *akt2* knockout mice among many other phenotypes have smaller BATs (Cho et
567 al., 2001; Garofalo et al., 2003).
568
569 An unexpected finding in our study is that all of the classic AKT substrates we
570 examined, whether in vitro in *Rictor*-deficient bAPCs or in vivo in mature *Rictor*-deficient
571 brown adipocytes, are phosphorylated normally. Why then does deleting *Rictor* in BAT
572 cause a metabolic shift? One possibility is that forkhead box O (FOXO) transcription factors
573 are more active in Rictor-deficient brown adipocytes. FOXOs are regulated by multiple
574 signals and function as cellular homeostasis regulators under stressful conditions
575 (Eijkelenboom and Burgering, 2013). FoxO1 and FoxO3 are classic AKT substrates
576 inhibited by AKT phosphorylation (through 14-3-3 mediated cytoplasmic retention) that
577 are partially dephosphorylated in some Rictor-deficient cell types (Guertin et al., 2009;
578 Guertin et al., 2006; Hagiwara et al., 2012; Jacinto et al., 2006; Yuan et al., 2012). When
579 FoxO1 and FoxO3 are dephosphorylated, they translocate to the nucleus where, thorough
580 poorly understood mechanisms operating in a cell-type specific manners, they affect
581 metabolism, survival, and cell cycle genes (including *Ucp1*) and the activity of
582 transcriptional regulators (including PPARγ and C/EBPα) (Eijkelenboom and Burgering,
583 2013; Ortega-Molina et al., 2012). However, FoxO1/3 phosphorylation is not affected in
584 Rictor-deficient BAT; thus, if the metabolic shift is driven by FOXOs, it may be through an

585 alterative mechanism such as acetylation (Banks et al., 2011; Masui et al., 2013). Another
586 possibility is that FoxC2 mediates the metabolic shift (Cederberg et al., 2001; Yao et al.,
587 2013); however, we do not observe any change in FoxC2 expression in *Rictor*-deficient
588 preadipocytes (not shown), nor do we see effects on the FoxC2 targets *C/ebpβ* or *Wnt10b*
589 during differentiation (Gerin et al., 2009). The most interesting possibility is that the shift
590 is mediated through an unidentified AKT pathway. Whatever the reason, why it differs
591 from other AKT pathways and uniquely requires hydrophobic motif phosphorylation is not
592 clear. This is an important ongoing area of investigation.
593
594 Consistent with the *Myf5*-lineage giving rise to a subset of white adipocytes, we also
595 uncovered an essential role for Rictor/mTORC2 in vivo in white adipocyte growth. This
596 confirms our previous discovery that some white adipocytes arise from *Myf5-cre*
597 expressing precursors (Sanchez-Gurmaches and Guertin, 2014b; Sanchez-Gurmaches et al.,
598 2012). However, because in the $Rictor^{Myf5cKO}$ mice the Rictor-deficient white adipocytes are
599 interspersed heterogeneously with non-deleted adipocytes within the same depot, we
600 could not perform the appropriate whole-tissue biochemical studies using Rictor-deficient
601 WAT. We did however determine that $Rictor^{iKO}$ white adipocyte precursors purified from
602 the stromal vascular fraction of psWAT (which are not *Myf5*-lineage derived) are also
603 defective at differentiating in vitro (not shown) indicating Rictor also has a cell
604 autonomous role in white adipocyte differentiation that is not dependent upon being *Myf5*-
605 lineage derived. To determine the in vivo relevance of these findings we will need to
606 identify Cre drivers that express uniformly and specifically in white adipocyte precursors;
607 however, the origins of adipocytes are just beginning to be revealed and appropriate tools
608 are not yet available for this line of investigation.
609
610 Is Rictor/mTORC2 a master regulator of lipid metabolism? Recent studies of liver
611 collectively report that deleting hepatic *Rictor* results in a complex phenotype including
612 increased gluconeogenesis, decreased glycolysis, and impaired lipogenesis (Hagiwara et al.,
613 2012; Lamming et al., 2012; Yuan et al., 2012). Two studies find that hepatic *Rictor* loss
614 also decreases SREBP1c activity; however, one study suggests AKT2 mediates this function

615 (Hagiwara et al., 2012) while the other proposes an AKT-independent pathway (Yuan et al.,
616 2012). These two studies are also inconsistent with respect to how *Rictor* loss affects AKT
617 signaling and thus the role of hepatic Rictor/mTORC2 is currently controversial.
618 Nevertheless, the glucose uptake and glycolysis defect is reportedly independent of the
619 lipogenesis defect because restoring glucose flux in *Rictor*-KO hepatocytes did not rescue
620 lipogenesis (Hagiwara et al., 2012). This study also reports that fatty acid oxidation genes
621 are elevated in Rictor-deficient hepatocytes (Hagiwara et al., 2012). Thus, Rictor/mTORC2
622 may have a broad role in establishing a pro-lipogenic metabolic state. Going forward it is
623 important to determine if Rictor/mTORC2 regulates de novo lipogenesis and beta-
624 oxidation by a common or coordinate set of mechanisms, or whether one metabolic
625 deficiency is indirectly driving the other. Notably, we detect a decrease in lipogenesis gene
626 expression in P1 BAT lacking Rictor, but the increase in fatty acid oxidation gene
627 expression we first detect in 6-week mutant BAT. Thus, mitochondrial activity may
628 progressively increase in the Rictor-deficient BAT and be secondary to a lipogenesis defect.
629 Regardless, our findings support the idea that targeting lipogenesis and/or beta-oxidation
630 pathways could be one approach to treating obesity and diabetes.
631
632 Obesity develops when energy intake exceeds expenditure and one prediction is
633 that increasing BAT energy expenditure could have anti-obesity therapeutic potential
634 (Tseng et al., 2010). To achieve this goal, a much deeper understanding of how BAT utilizes
635 fuel is required (Townsend and Tseng, 2014). An important finding in our study is that
636 $Rictor^{Myf5cKO}$ mice living at thermoneutrality, when challenged with an obesogenic diet,
637 induce higher levels of UCP1 and are more resistant to developing obesity and metabolic
638 disease compared to HFD-fed controls. This suggests that inhibiting mTORC2 in BAT
639 augments diet-induced thermogenesis (Cannon and Nedergaard, 2010; Feldmann et al.,
640 2009); however, we cannot yet rule out that Rictor loss in other *Myf5*-lineage tissues might
641 contribute to this phenotype. It is currently being debated as to whether humans have
642 classic brown adipocytes or a potential third class of adipocyte called a brite/beige
643 adipocyte (Nedergaard and Cannon, 2013). Recent work indicates that in the neck, deep fat
644 is similar to rodent BAT and expresses high levels of UCP1 while more superficial fat
645 expresses lower UCP1 levels and has more brite/beige characteristics (Cypess et al., 2013).

Notably, humans typically adjust temperature to be at or around thermoneutrality (Cannon and Nedergaard, 2010), and interestingly the BAT of mice living at thermoneutrality is "humanized"; that is appearing more "white-fat like", or perhaps more "brite/beige-fat" like [Figure 7]. Thus, it seems likely that humans possess classic brown fat and that studies of brown fat in mice will provide important insights into human BAT regulation. Continued elucidation of mTORC2 pathways in BAT bioenergetics could therefore lead to novel human anti-obesity therapies that target cellular energy expenditure.

EXPERIMENTAL PROCEDURES

Antibodies and reagents

Rictor (Cat# 2140), mTOR (2983), pan-AKT (9272), GSK3β (9315), ACC (3676), ACLY (4332), NDRG1 (9408) and β-actin (4970), Insulin receptor β (3025) and anti-HA-tag (2367) antibodies were purchased from Cell Signaling Technologies. SREBP1 (sc-366), p70 S6K (sc-9027), UCP1 antibody (sc-6528), and HRP-conjugated secondary antibodies were from Santa Cruz biotechnology. All phosphorylation-specific antibodies: S473-AKT (4058), T308-AKT (4056), T24-FoxO1 (9464), S9-GSK3β (9323), T1462-TSC2 (3617) and T389-S6K (9234) were from Cell Signaling Technologies. 4-hydroxy-tamoxifen (4-OHT) was from Toronto Research Chemicals. Indomethacin, dexamethasone, 3-isobutyl-1-methylxanthine (IBMX) and all other reagents were from Sigma-Aldrich.

Plasmids

Full length AKT1 cDNA obtained by PCR amplification from pcDNA3-myr-HA-AKT1 (addgene #9008) was subcloned into the pCMV-HA vector. Full length AKT2 cDNA obtained by PCR amplification from pBabe-myr-HA-AKT2 (addgene #9018) was subcloned into the pCMV-HA vector. SGK1 cDNA (Thermo Scientific #MHS6278-202755905) was PCR amplified to obtain a truncated SGK sequence (SGK-delta-60N, N-terminal 1-60 amino acids deletion). Phosphomimetic constructs with indicated mutation were done by QuikChange Site-Directed Mutagenesis kit (Stratagene) with appropriate primers. All cDNA constructs were also transferred into pBabe-puro retroviral vector for stable expression.

Mice

Rictor floxed (*Rictor*$^{fl/fl}$) mice (Shiota et al., 2006) or *Raptor*$^{fl/fl}$ mice (Peterson et al., 2011) were crossed with *Myf5-cre* (JAX #007893)(Tallquist et al., 2000), *Ubc-CreERT2* (JAX #007001)(Ruzankina et al., 2007) and *Pax7-CreERT2* (JAX #012476)(Lepper et al., 2009), to make conditional or inducible knockout mice. *Rosa26-mTmG* (JAX #007676) and *Rosa26–LSL-LacZ* (JAX #003474) were also obtained from Jackson laboratory. Male 129/C57B6 mice were used for all studies.

Satellite cells isolation and differentiation

Adult muscle satellite cells were isolated according to (Sherwood et al., 2004). See also Supplemental Experimental Procedures.

Gene Expression and qRT-PCR array

Total RNA was isolated from cells or tissues using Qiazol (Invitrogen) and an RNeasy kit (Invitrogen). Equal amounts of RNA from each individual sample were retro-transcribed to cDNA using a High capacity cDNA reverse transcription kit (Applied Biosystems). *Tbp* expression was used as a normalization gene in most RT-PCR experiments. A different set of iBAT samples was used in RT-PCR arrays (Qiagen) according to manufacturer's instruction. See also Supplemental Experimental Procedures.

Brown preadipocytes and in vitro differentiation

Primary brown adipocyte precursors (bAPC) cells were isolated from P1 neonates and immortalized with pBabe-SV40 Large T antigen. To induce *Rictor* deletion *ubc-creERT2;Rictor*$^{fl/fl}$ cells were treated on three consecutive days with 1μM 4-OHT. bAPCs were seeded at $4x10^4$ cells/ml and allowed reach confluence over 3 days in media containing 20nM insulin, 1nM T3 (differentiation medium). On day 4, cells were induced with 20nM insulin, 1nM T3, 0.125mM indomethacin, 2μg/mL dexamethasone and 0.5mM 3-isobutyl-1-methylxanthine (IBMX). Two days later the induction medium was replaced with fresh differentiation medium and changed every two days until day 10. See also Supplemental Experimental Procedures.

***Ex vivo* oxygen consumption**

Brown adipose tissue oxygen consumption rate was measured with a Seahorse Analyzer according to a previous published protocol (Vernochet et al., 2012). See also Supplemental Experimental Procedures.

Metabolic studies

For thermoneutrality studies, 6 week-old male mice were transferred to the mouse room with elevated housing temperature (30°C). Mice were kept one week in thermoneutrality

before using in any experiment. At 7 weeks of age, mice were started to receiving chow diet (Prolab Isopro RMH3000, LabDiet) or high fat diet (45% calories from fat; ResearchDiet # D12451). Mouse body weight and food intake were accessed weekly for 12 weeks. Glucose tolerance tests were performed at the 11^{th} week of the diet experiment. Overnight fasted animals were subjected to GTT by i.p. injecting glucose at 2g/Kg of body weight and blood glucose levels were measured by a commercially available glucose meter. A small group (n=4) of mice were kept for 20 weeks of HFD for morphological studies.

Statistics

Unless otherwise stated, the results are described as mean ± SEM. Two-way ANOVA was performed where indicated. For most experiments Student's t-test was used to determine statistical significance: *indicates $P<0.05$; **, $P<0.01$; ***, $P<0.001$.

See also Supplemental Experimental Procedures

AUTHOR CONTRIBUTIONS

C-M.H. and D.A.G. conceived the project, designed the experiments, and wrote and edited the manuscript. C-M.H. performed most of the experiments and D.A.G. assisted in the analysis and interpretation. C.M.C. assisted with the PPARγ rescue experiments. J.S-G. assisted with the lineage tracing experiments. H.L. helped with animal experiments. C.B.C. performed metabolite profiling and analysis. S.H. and A.J.W. assisted with the satellite cell isolation and muscle regeneration experiments.

ACKNOWLEDGEMENTS

This work was supported by grants from the National Institutes of Health (R00CA129613 & R01DK094004), the American Diabetes Association (ADA113BS-066), and awards from the Pew Charitable Trusts and Charles Hood Foundation to D.A.G. We thank Yuefeng Tang, Xiaohao Yao, and Christine Powers for technical assistance, Morris Birnbaum for providing *Akt*1&2 floxed mice, and Marcus Cooper for the PPARγ2 construct. Metabolic cage studies were performed in the UMass Mouse Phenotype Center (DK09300). The authors declare no conflict of interests.

REFERENCES

Balcke, G.U., Kolle, S.N., Kamp, H., Bethan, B., Looser, R., Wagner, S., Landsiedel, R., and van Ravenzwaay, B. (2011). Linking energy metabolism to dysfunctions in mitochondrial respiration--a metabolomics in vitro approach. Toxicology letters 203, 200-209.

Banks, A.S., Kim-Muller, J.Y., Mastracci, T.L., Kofler, N.M., Qiang, L., Haeusler, R.A., Jurczak, M.J., Laznik, D., Heinrich, G., Samuel, V.T., Shulman, G.I., Papaioannou, V.E., and Accili, D. (2011). Dissociation of the glucose and lipid regulatory functions of FoxO1 by targeted knockin of acetylation-defective alleles in mice. Cell metabolism 14, 587-597.

Ben-Sahra, I., Howell, J.J., Asara, J.M., and Manning, B.D. (2013). Stimulation of de Novo Pyrimidine Synthesis by Growth Signaling Through mTOR and S6K1. Science.

Bentzinger, C.F., Romanino, K., Cloetta, D., Lin, S., Mascarenhas, J.B., Oliveri, F., Xia, J., Casanova, E., Costa, C.F., Brink, M., Zorzato, F., Hall, M.N., and Ruegg, M.A. (2008). Skeletal muscle-specific ablation of raptor, but not of rictor, causes metabolic changes and results in muscle dystrophy. Cell metabolism 8, 411-424.

Cannon, B., and Nedergaard, J. (2004). Brown adipose tissue: function and physiological significance. Physiological reviews 84, 277-359.

Cannon, B., and Nedergaard, J. (2010). Metabolic consequences of the presence or absence of the thermogenic capacity of brown adipose tissue in mice (and probably in humans). Int J Obes (Lond) 34 Suppl 1, S7-16.

Cederberg, A., Gronning, L.M., Ahren, B., Tasken, K., Carlsson, P., and Enerback, S. (2001). FOXC2 is a winged helix gene that counteracts obesity, hypertriglyceridemia, and diet-induced insulin resistance. Cell 106, 563-573.

Cho, H., Mu, J., Kim, J.K., Thorvaldsen, J.L., Chu, Q., Crenshaw, E.B., 3rd, Kaestner, K.H., Bartolomei, M.S., Shulman, G.I., and Birnbaum, M.J. (2001). Insulin resistance and a diabetes mellitus-like syndrome in mice lacking the protein kinase Akt2 (PKB beta). Science 292, 1728-1731.

Cristancho, A.G., and Lazar, M.A. (2011). Forming functional fat: a growing understanding of adipocyte differentiation. Nature reviews. Molecular cell biology 12, 722-734.

Cybulski, N., Polak, P., Auwerx, J., Ruegg, M.A., and Hall, M.N. (2009). mTOR complex 2 in adipose tissue negatively controls whole-body growth. Proceedings of the National Academy of Sciences of the United States of America 106, 9902-9907.

Cypess, A.M., Lehman, S., Williams, G., Tal, I., Rodman, D., Goldfine, A.B., Kuo, F.C., Palmer, E.L., Tseng, Y.H., Doria, A., Kolodny, G.M., and Kahn, C.R. (2009). Identification and importance of brown adipose tissue in adult humans. The New England journal of medicine 360, 1509-1517.

792 Cypess, A.M., White, A.P., Vernochet, C., Schulz, T.J., Xue, R., Sass, C.A., Huang, T.L., Roberts-
793 Toler, C., Weiner, L.S., Sze, C., Chacko, A.T., Deschamps, L.N., Herder, L.M., Truchan, N.,
794 Glasgow, A.L., Holman, A.R., Gavrila, A., Hasselgren, P.O., Mori, M.A., Molla, M., and Tseng,
795 Y.H. (2013). Anatomical localization, gene expression profiling and functional
796 characterization of adult human neck brown fat. Nature medicine 19, 635-639.

797 Czech, M.P., Tencerova, M., Pedersen, D.J., and Aouadi, M. (2013). Insulin signalling
798 mechanisms for triacylglycerol storage. Diabetologia.

799 Eijkelenboom, A., and Burgering, B.M. (2013). FOXOs: signalling integrators for
800 homeostasis maintenance. Nature reviews. Molecular cell biology 14, 83-97.

801 Fasshauer, M., Klein, J., Kriauciunas, K.M., Ueki, K., Benito, M., and Kahn, C.R. (2001).
802 Essential role of insulin receptor substrate 1 in differentiation of brown adipocytes.
803 Molecular and cellular biology 21, 319-329.

804 Feldmann, H.M., Golozoubova, V., Cannon, B., and Nedergaard, J. (2009). UCP1 ablation
805 induces obesity and abolishes diet-induced thermogenesis in mice exempt from thermal
806 stress by living at thermoneutrality. Cell metabolism 9, 203-209.

807 Filhoulaud, G., Guilmeau, S., Dentin, R., Girard, J., and Postic, C. (2013). Novel insights into
808 ChREBP regulation and function. Trends in endocrinology and metabolism: TEM 24, 257-
809 268.

810 Garcia-Martinez, J.M., and Alessi, D.R. (2008). mTOR complex 2 (mTORC2) controls
811 hydrophobic motif phosphorylation and activation of serum- and glucocorticoid-induced
812 protein kinase 1 (SGK1). The Biochemical journal 416, 375-385.

813 Garofalo, R.S., Orena, S.J., Rafidi, K., Torchia, A.J., Stock, J.L., Hildebrandt, A.L., Coskran, T.,
814 Black, S.C., Brees, D.J., Wicks, J.R., McNeish, J.D., and Coleman, K.G. (2003). Severe diabetes,
815 age-dependent loss of adipose tissue, and mild growth deficiency in mice lacking Akt2/PKB
816 beta. J Clin Invest 112, 197-208.

817 Gerin, I., Bommer, G.T., Lidell, M.E., Cederberg, A., Enerback, S., and Macdougald, O.A.
818 (2009). On the role of FOX transcription factors in adipocyte differentiation and insulin-
819 stimulated glucose uptake. The Journal of biological chemistry 284, 10755-10763.

820 Gesta, S., Tseng, Y.H., and Kahn, C.R. (2007). Developmental origin of fat: tracking obesity to
821 its source. Cell 131, 242-256.

822 Guertin, D.A., Stevens, D.M., Saitoh, M., Kinkel, S., Crosby, K., Sheen, J.H., Mullholland, D.J.,
823 Magnuson, M.A., Wu, H., and Sabatini, D.M. (2009). mTOR complex 2 is required for the
824 development of prostate cancer induced by Pten loss in mice. Cancer cell 15, 148-159.

825 Guertin, D.A., Stevens, D.M., Thoreen, C.C., Burds, A.A., Kalaany, N.Y., Moffat, J., Brown, M.,
826 Fitzgerald, K.J., and Sabatini, D.M. (2006). Ablation in mice of the mTORC components

827 raptor, rictor, or mLST8 reveals that mTORC2 is required for signaling to Akt-FOXO and
828 PKCalpha, but not S6K1. Developmental cell 11, 859-871.

829 Hagiwara, A., Cornu, M., Cybulski, N., Polak, P., Betz, C., Trapani, F., Terracciano, L., Heim,
830 M.H., Ruegg, M.A., and Hall, M.N. (2012). Hepatic mTORC2 Activates Glycolysis and
831 Lipogenesis through Akt, Glucokinase, and SREBP1c. Cell metabolism 15, 725-738.

832 Harms, M., and Seale, P. (2013). Brown and beige fat: development, function and
833 therapeutic potential. Nature medicine 19, 1252-1263.

834 Harms, M.J., Ishibashi, J., Wang, W., Lim, H.W., Goyama, S., Sato, T., Kurokawa, M., Won, K.J.,
835 and Seale, P. (2014). Prdm16 is required for the maintenance of brown adipocyte identity
836 and function in adult mice. Cell metabolism 19, 593-604.

837 Infantino, V., Iacobazzi, V., De Santis, F., Mastrapasqua, M., and Palmieri, F. (2007).
838 Transcription of the mitochondrial citrate carrier gene: role of SREBP-1, upregulation by
839 insulin and downregulation by PUFA. Biochemical and biophysical research
840 communications 356, 249-254.

841 Jacinto, E., Facchinetti, V., Liu, D., Soto, N., Wei, S., Jung, S.Y., Huang, Q., Qin, J., and Su, B.
842 (2006). SIN1/MIP1 maintains rictor-mTOR complex integrity and regulates Akt
843 phosphorylation and substrate specificity. Cell 127, 125-137.

844 Kajimura, S., Seale, P., and Spiegelman, B.M. (2010). Transcriptional control of brown fat
845 development. Cell metabolism 11, 257-262.

846 Kumar, A., Harris, T.E., Keller, S.R., Choi, K.M., Magnuson, M.A., and Lawrence, J.C., Jr. (2008).
847 Muscle-specific deletion of rictor impairs insulin-stimulated glucose transport and
848 enhances Basal glycogen synthase activity. Molecular and cellular biology 28, 61-70.

849 Kumar, A., Lawrence, J.C., Jr., Jung, D.Y., Ko, H.J., Keller, S.R., Kim, J.K., Magnuson, M.A., and
850 Harris, T.E. (2010). Fat cell-specific ablation of rictor in mice impairs insulin-regulated fat
851 cell and whole-body glucose and lipid metabolism. Diabetes 59, 1397-1406.

852 Lamming, D.W., Ye, L., Katajisto, P., Goncalves, M.D., Saitoh, M., Stevens, D.M., Davis, J.G.,
853 Salmon, A.B., Richardson, A., Ahima, R.S., Guertin, D.A., Sabatini, D.M., and Baur, J.A. (2012).
854 Rapamycin-induced insulin resistance is mediated by mTORC2 loss and uncoupled from
855 longevity. Science 335, 1638-1643.

856 Laplante, M., and Sabatini, D.M. (2012). mTOR Signaling in Growth Control and Disease. Cell
857 149, 274-293.

858 Lee, K.Y., Russell, S.J., Ussar, S., Boucher, J., Vernochet, C., Mori, M.A., Smyth, G., Rourk, M.,
859 Cederquist, C., Rosen, E.D., Kahn, B.B., and Kahn, C.R. (2013). Lessons on conditional gene
860 targeting in mouse adipose tissue. Diabetes 62, 864-874.

Lepper, C., Conway, S.J., and Fan, C.M. (2009). Adult satellite cells and embryonic muscle progenitors have distinct genetic requirements. Nature 460, 627-631.

Martinez-Lopez, N., Athonvarangkul, D., Sahu, S., Coletto, L., Zong, H., Bastie, C.C., Pessin, J.E., Schwartz, G.J., and Singh, R. (2013). Autophagy in Myf5+ progenitors regulates energy and glucose homeostasis through control of brown fat and skeletal muscle development. EMBO reports 14, 795-803.

Masui, K., Tanaka, K., Akhavan, D., Babic, I., Gini, B., Matsutani, T., Iwanami, A., Liu, F., Villa, G.R., Gu, Y., Campos, C., Zhu, S., Yang, H., Yong, W.H., Cloughesy, T.F., Mellinghoff, I.K., Cavenee, W.K., Shaw, R.J., and Mischel, P.S. (2013). mTOR Complex 2 Controls Glycolytic Metabolism in Glioblastoma through FoxO Acetylation and Upregulation of c-Myc. Cell metabolism.

Mizuarai, S., Miki, S., Araki, H., Takahashi, K., and Kotani, H. (2005). Identification of dicarboxylate carrier Slc25a10 as malate transporter in de novo fatty acid synthesis. The Journal of biological chemistry 280, 32434-32441.

Mullican, S.E., Tomaru, T., Gaddis, C.A., Peed, L.C., Sundaram, A., and Lazar, M.A. (2013). A novel adipose-specific gene deletion model demonstrates potential pitfalls of existing methods. Mol Endocrinol 27, 127-134.

Muzumdar, M.D., Tasic, B., Miyamichi, K., Li, L., and Luo, L. (2007). A global double-fluorescent Cre reporter mouse. Genesis 45, 593-605.

Nedergaard, J., Bengtsson, T., and Cannon, B. (2007). Unexpected evidence for active brown adipose tissue in adult humans. Am J Physiol Endocrinol Metab 293, E444-452.

Nedergaard, J., and Cannon, B. (2010). The changed metabolic world with human brown adipose tissue: therapeutic visions. Cell metabolism 11, 268-272.

Nedergaard, J., and Cannon, B. (2013). How brown is brown fat? It depends where you look. Nature medicine 19, 540-541.

Ohno, H., Shinoda, K., Ohyama, K., Sharp, L.Z., and Kajimura, S. (2013). EHMT1 controls brown adipose cell fate and thermogenesis through the PRDM16 complex. Nature 504, 163-167.

Ortega-Molina, A., Efeyan, A., Lopez-Guadamillas, E., Munoz-Martin, M., Gomez-Lopez, G., Canamero, M., Mulero, F., Pastor, J., Martinez, S., Romanos, E., Mar Gonzalez-Barroso, M., Rial, E., Valverde, A.M., Bischoff, J.R., and Serrano, M. (2012). Pten positively regulates brown adipose function, energy expenditure, and longevity. Cell metabolism 15, 382-394.

Pearce, L.R., Komander, D., and Alessi, D.R. (2010). The nuts and bolts of AGC protein kinases. Nature reviews. Molecular cell biology 11, 9-22.

Peterson, T.R., Sengupta, S.S., Harris, T.E., Carmack, A.E., Kang, S.A., Balderas, E., Guertin, D.A., Madden, K.L., Carpenter, A.E., Finck, B.N., and Sabatini, D.M. (2011). mTOR complex 1 regulates lipin 1 localization to control the SREBP pathway. Cell 146, 408-420.

Robitaille, A.M., Christen, S., Shimobayashi, M., Cornu, M., Fava, L.L., Moes, S., Prescianotto-Baschong, C., Sauer, U., Jenoe, P., and Hall, M.N. (2013). Quantitative Phosphoproteomics Reveal mTORC1 Activates de Novo Pyrimidine Synthesis. Science.

Ruzankina, Y., Pinzon-Guzman, C., Asare, A., Ong, T., Pontano, L., Cotsarelis, G., Zediak, V.P., Velez, M., Bhandoola, A., and Brown, E.J. (2007). Deletion of the developmentally essential gene ATR in adult mice leads to age-related phenotypes and stem cell loss. Cell stem cell 1, 113-126.

Sanchez-Gurmaches, J., and Guertin, D.A. (2014a). Adipocyte lineages: tracing back the origins of fat. Biochimica et biophysica acta 1842, 340-351.

Sanchez-Gurmaches, J., and Guertin, D.A. (2014b). Adipocytes arise from multiple lineages that are heterogeneously and dynamically distributed. Nature communications in press.

Sanchez-Gurmaches, J., Hung, C.M., Sparks, C.A., Tang, Y., Li, H., and Guertin, D.A. (2012). PTEN loss in the Myf5 lineage redistributes body fat and reveals subsets of white adipocytes that arise from Myf5 precursors. Cell metabolism 16, 348-362.

Sarbassov, D.D., Guertin, D.A., Ali, S.M., and Sabatini, D.M. (2005). Phosphorylation and regulation of Akt/PKB by the rictor-mTOR complex. Science 307, 1098-1101.

Schulz, T.J., Huang, P., Huang, T.L., Xue, R., McDougall, L.E., Townsend, K.L., Cypess, A.M., Mishina, Y., Gussoni, E., and Tseng, Y.H. (2013). Brown-fat paucity due to impaired BMP signalling induces compensatory browning of white fat. Nature 495, 379-383.

Schulz, T.J., and Tseng, Y.H. (2013). Brown adipose tissue: development, metabolism and beyond. The Biochemical journal 453, 167-178.

Seale, P., Bjork, B., Yang, W., Kajimura, S., Chin, S., Kuang, S., Scime, A., Devarakonda, S., Conroe, H.M., Erdjument-Bromage, H., Tempst, P., Rudnicki, M.A., Beier, D.R., and Spiegelman, B.M. (2008). PRDM16 controls a brown fat/skeletal muscle switch. Nature 454, 961-967.

Sherwood, R.I., Christensen, J.L., Conboy, I.M., Conboy, M.J., Rando, T.A., Weissman, I.L., and Wagers, A.J. (2004). Isolation of adult mouse myogenic progenitors: functional heterogeneity of cells within and engrafting skeletal muscle. Cell 119, 543-554.

Shiota, C., Woo, J.T., Lindner, J., Shelton, K.D., and Magnuson, M.A. (2006). Multiallelic disruption of the rictor gene in mice reveals that mTOR complex 2 is essential for fetal growth and viability. Developmental cell 11, 583-589.

929 Tallquist, M.D., Weismann, K.E., Hellstrom, M., and Soriano, P. (2000). Early myotome
930 specification regulates PDGFA expression and axial skeleton development. Development
931 127, 5059-5070.

932 Townsend, K.L., and Tseng, Y.H. (2014). Brown fat fuel utilization and thermogenesis.
933 Trends in endocrinology and metabolism: TEM 25, 168-177.

934 Tseng, Y.H., Butte, A.J., Kokkotou, E., Yechoor, V.K., Taniguchi, C.M., Kriauciunas, K.M.,
935 Cypess, A.M., Niinobe, M., Yoshikawa, K., Patti, M.E., and Kahn, C.R. (2005). Prediction of
936 preadipocyte differentiation by gene expression reveals role of insulin receptor substrates
937 and necdin. Nature cell biology 7, 601-611.

938 Tseng, Y.H., Cypess, A.M., and Kahn, C.R. (2010). Cellular bioenergetics as a target for
939 obesity therapy. Nature reviews. Drug discovery 9, 465-482.

940 Tseng, Y.H., Kokkotou, E., Schulz, T.J., Huang, T.L., Winnay, J.N., Taniguchi, C.M., Tran, T.T.,
941 Suzuki, R., Espinoza, D.O., Yamamoto, Y., Ahrens, M.J., Dudley, A.T., Norris, A.W., Kulkarni,
942 R.N., and Kahn, C.R. (2008). New role of bone morphogenetic protein 7 in brown
943 adipogenesis and energy expenditure. Nature 454, 1000-1004.

944 van Marken Lichtenbelt, W.D., Vanhommerig, J.W., Smulders, N.M., Drossaerts, J.M.,
945 Kemerink, G.J., Bouvy, N.D., Schrauwen, P., and Teule, G.J. (2009). Cold-activated brown
946 adipose tissue in healthy men. The New England journal of medicine 360, 1500-1508.

947 Vernochet, C., Mourier, A., Bezy, O., Macotela, Y., Boucher, J., Rardin, M.J., An, D., Lee, K.Y.,
948 Ilkayeva, O.R., Zingaretti, C.M., Emanuelli, B., Smyth, G., Cinti, S., Newgard, C.B., Gibson, B.W.,
949 Larsson, N.G., and Kahn, C.R. (2012). Adipose-specific deletion of TFAM increases
950 mitochondrial oxidation and protects mice against obesity and insulin resistance. Cell
951 metabolism 16, 765-776.

952 Virtanen, K.A., Lidell, M.E., Orava, J., Heglind, M., Westergren, R., Niemi, T., Taittonen, M.,
953 Laine, J., Savisto, N.J., Enerback, S., and Nuutila, P. (2009). Functional brown adipose tissue
954 in healthy adults. The New England journal of medicine 360, 1518-1525.

955 Walden, T.B., Hansen, I.R., Timmons, J.A., Cannon, B., and Nedergaard, J. (2011). Recruited
956 versus nonrecruited molecular signatures of brown, "brite" and white adipose tissues. Am J
957 Physiol Endocrinol Metab.

958 Wang, F., Mullican, S.E., DiSpirito, J.R., Peed, L.C., and Lazar, M.A. (2013). Lipoatrophy and
959 severe metabolic disturbance in mice with fat-specific deletion of PPARgamma.
960 Proceedings of the National Academy of Sciences of the United States of America 110,
961 18656-18661.

962 Yao, Y., Suraokar, M., Darnay, B.G., Hollier, B.G., Shaiken, T.E., Asano, T., Chen, C.H., Chang,
963 B.H., Lu, Y., Mills, G.B., Sarbassov, D., Mani, S.A., Abbruzzese, J.L., and Reddy, S.A. (2013).
964 BSTA promotes mTORC2-mediated phosphorylation of Akt1 to suppress expression of
965 FoxC2 and stimulate adipocyte differentiation. Science signaling 6, ra2.

966 Yuan, M., Pino, E., Wu, L., Kacergis, M., and Soukas, A.A. (2012). Identification of Akt-
967 independent regulation of hepatic lipogenesis by mammalian target of rapamycin (mTOR)
968 complex 2. The Journal of biological chemistry 287, 29579-29588.
969
970

FIGURE LEGENDS

Figure 1. Post-natal brown and white adipose tissue growth requires Rictor

(A) Growth curve of control and *Rictor*^{Myf5cKO} mice (n=13; bars represent mean ± SEM; t-test; *p<0.05, **p<0.01, ***p<0.001).

(B) (Left) Mass of BATs as a percent of total body weight (6-wks) (n=19-21; bars represent mean ± SEM; t-test; ***p<0.001) and (Right) representative image of control and mutant iBAT (6-wks).

(C) (Left) Mass of WATs expressed as a percent of total body weight (6-wks) (n=14-16; bars represent mean ± SEM; t-test; **p<0.01, ***p<0.001) and (Right) representative image of control and mutant rWAT (6-wks).

(D) Mass of lean tissues expressed as a percent of total body weight (6-wks) (n=15-19; bars represent mean ± SEM; t-test; ***p<0.001).

(E) Western blots of lysates prepared from the indicated tissues (6-wks).

(F) Tissue mass expressed as average weight (mg) at 6-wks and 6-mos of age (n= 14-21 for 6-wks mice; n=7 for 6-mos mice; bars represent mean ± SEM; t-test; ***p<0.001).

See also Figure S1.

Figure 2. Brown and white adipocytes lacking *Rictor* are smaller and multilocular

(A) H&E stains of interscapular brown adipose tissue (iBAT) at embryonic day 18.5 (E18.5), postnatal day 1 (P1), 6 week (6 w) and 6 months (6 m).

(B) H&E stains of retroperitoneal (rWAT) and anterior subcutaneous (asWAT) at 6-wks.

(C) Representative images of mTFP and mGFP labeled rWAT and asWAT adipocytes. Enlarged images are indicated by white box at 63X.

See also Figure S2.

Figure 3. Rictor-deficient brown adipocytes have a lipid metabolism defect despite having normal pan-AKT signaling

(A) Western blots of the indicated total and phospho-proteins using 6-wks iBAT lysates. Mice were fasted overnight and re-fed for 45mins prior to preparing lysates.

(B-D) qRT-PCR of the indicated genes in P1 (n=6) and 6wk (n=8) iBAT (bars represent mean ± SEM; t-test; *p<0.05, **p<0.01)
See also Figure S3.

Figure 4. Mitochondrial activity is elevated in Rictor-deficient BAT

(A) qRT-PCR of mitochondrial genes in P1 (n=6) and 6wk iBAT (n=8) (bars represent mean ± SEM; t-test; *p<0.05, **p<0.01)
(B) Differentially expressed mitochondrial functional genes found using qRT-PCR arrays. Data is shown as fold regulation (conditional KO relative to control) and all genes listed are significantly different between 6wk *control* and *Rictor*^{my5cKO} iBAT (n=4; t-test; p<0.05)
(C) Representative immunofluorescence images of mitochondrial Cox IV staining in 6wk iBAT (n=3).
(D) (Left) Representative TEM images of 6wk iBAT and (Right) quantification of mitochondria size (n=3; bars represent mean ± SEM; t-test; ***p<0.001)
(E) Oxygen consumption iBAT measured *ex vivo* using a Seahorse Flux Analyzer (12 wks, n=5; values are normalized to DNA content; bars represent mean ± SEM; t-test; *p<0.05)
(F) (Left) qRT-PCR of *Ucp1* mRNA expression in iBAT with or without cold exposure (n=3 for 22°C; n=4 for 4°C; bars represent mean ± SEM; two-way ANOVA; ***P<0.001) and (Right) rectal temperature in acute cold challenged mice (n=4; bars represent mean ± SEM; t-test; no significant difference).
See also Figure S4.

Figure 5. Rictor is required for brown adipocyte differentiation in vitro

(A) Western immunoblots showing phosphorylation of AKT and its effectors in control and *Rictor*^{iKO} brown preadipocytes. Cells were serum deprived for 3 hours then stimulated with 0, 5, 25, 120, or 600nM insulin respectively for 15 minutes prior to lysis.
(B) Oil Red O staining of control and *Rictor*^{iKO} cells after differentiation.
(C) Western immunoblots of the indicated total and phospho- proteins on each of the indicated days of differentiation.
(D) qRT-PCR of mRNA levels for the indicated differentiation-related genes (n=3; bars represent mean ± SEM; t-test; *p<0.05, ***p<0.001).

(E) Western immunoblots of the indicated total and phospho proteins on each of the indicated days of differentiation (samples correspond with panel (C)).
(F) Western immunoblots of cell lysates collected at day 10 of differentiation. M indicates mock transfection; V indicates cells transfected with empty vector; γ2 indicates cells transfected with recombinant PPARγ2. Arrows point to the γ1 and γ2 isoforms.
(G) Oil Red O staining of differentiated cells described in (F).
See also Figure S5.

Figure 6. Recombinant AKT1-S473D or BMP7 supplementation rescue differentiation in the absence of Rictor

(A) Oil Red O staining of differentiated control cells (vehicle-treated) and *Rictor*^{iKO} cells (4-OHT treated) that stably express the indicated recombinant constructs or empty vector.
(B) Western immunoblots of lysates prepared from the differentiated cells in (A).
(C) Western immunoblots of lysates prepared from undifferentiated control and *Rictor*^{iKO} cells. Cells were serum deprived for 3 hours, then stimulated with FBS or BMP7 (3.2nM) for 15 minutes.
(D) Oil Red O staining of differentiated control (vehicle-treated) and *Rictor*^{iKO} (4-OHT treated) cells in the presence or absence of BMP7. BMP7 (3.2nM) was added at day 1 in the differentiation protocol.
(E) Western immunoblots of lysates prepared from differentiated cells in (D).
See also Figure S6.

Figure 7. *Rictor*^{Myf5cKO} mice exempt from thermal stress and consuming a high fat diet are resistant to obesity and metabolic disease

(A) Weekly weight gain of control and *Rictor*^{Myf5cKO} mice during 12-weeks of each normal chow diet (chow) or high fat diet (HFD) (n=8 for control and n=12 for KO in chow; n=10 for both genotypes on HFD; bars represent mean ± SEM; t-test; *p<0.05) The control mice initially weighed 21.63±0.812g in the chow group and 21.24±0.621 in the HFD group; The *Rictor*^{Myf5cKO} mice initially weighted 19.42±0.305g in the chow group and 19.32±0.348 in the HFD group.

(B) Total energy intake (MJ) during the feeding regimen described in (A). Control mice consumed 3.75±0.557g of chow and 2.81±0.120g of HFD; *Rictor*^{Myf5cKO} mice consumed 3.85±0.237g of chow and 2.95±0.354g of HFD.

(C) Metabolic efficiency was determined as the amount of body weight increase (g) per MJ food consumed (n=8 for control and n=12 for KO on chow; n=10 for both genotypes on HFD; bars represent mean ± SEM; two-way *ANOVA*; *p<0.05, ***p<0.001).

(D) Mass (mg) of the indicated tissues collected from control and KO mice after 12 weeks on chow or HFD. (n=8 for control and n=12 for KO on chow; n=10 for both genotypes on HFD; bars represent mean ± SEM; two-way *ANOVA*; *p<0.05, ***p<0.001).

(E-F) H&E staining of iBAT and pgWAT and Oil red O staining of livers after 12-weeks of eating chow diet (E) or high fat diet (F).

(G) qRT-PCR of the indicated brown and white fat genes in iBAT from chow or HFD mice (n=8 for control and n=12 for KO on chow; n=10 for both genotypes on HFD; bars represent mean ± SEM; two-way *ANOVA*; *p<0.05, **p<0.01, ***p<0.001; # indicates significant difference over the control chow group).

(H) qRT-PCR of the indicated metabolic genes in iBAT from chow or HFD mice (n=8 for control and n=12 for KO in chow; n=10 for both genotypes in HFD; bars represent mean ± SEM; two-way *ANOVA*; *p<0.05, **p<0.01, ***p<0.001; # indicates significant difference over the control chow group).

(I) Western immunoblot for UCP1 and the indicated control proteins using lysates prepared from iBAT.

See also Figure S7.

Figure 1
Click here to download high resolution image

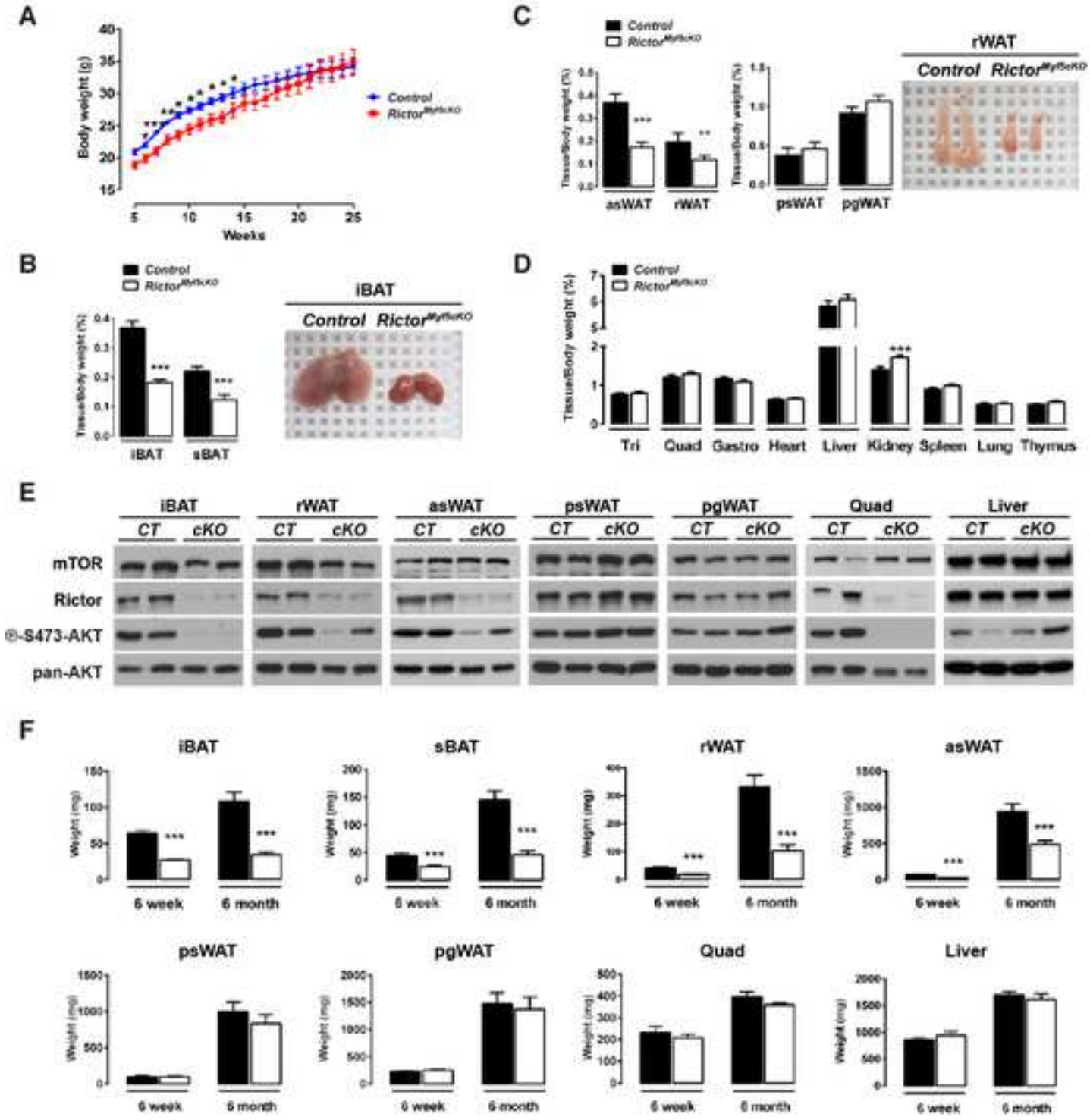

Figure 2

Click here to download high resolution image

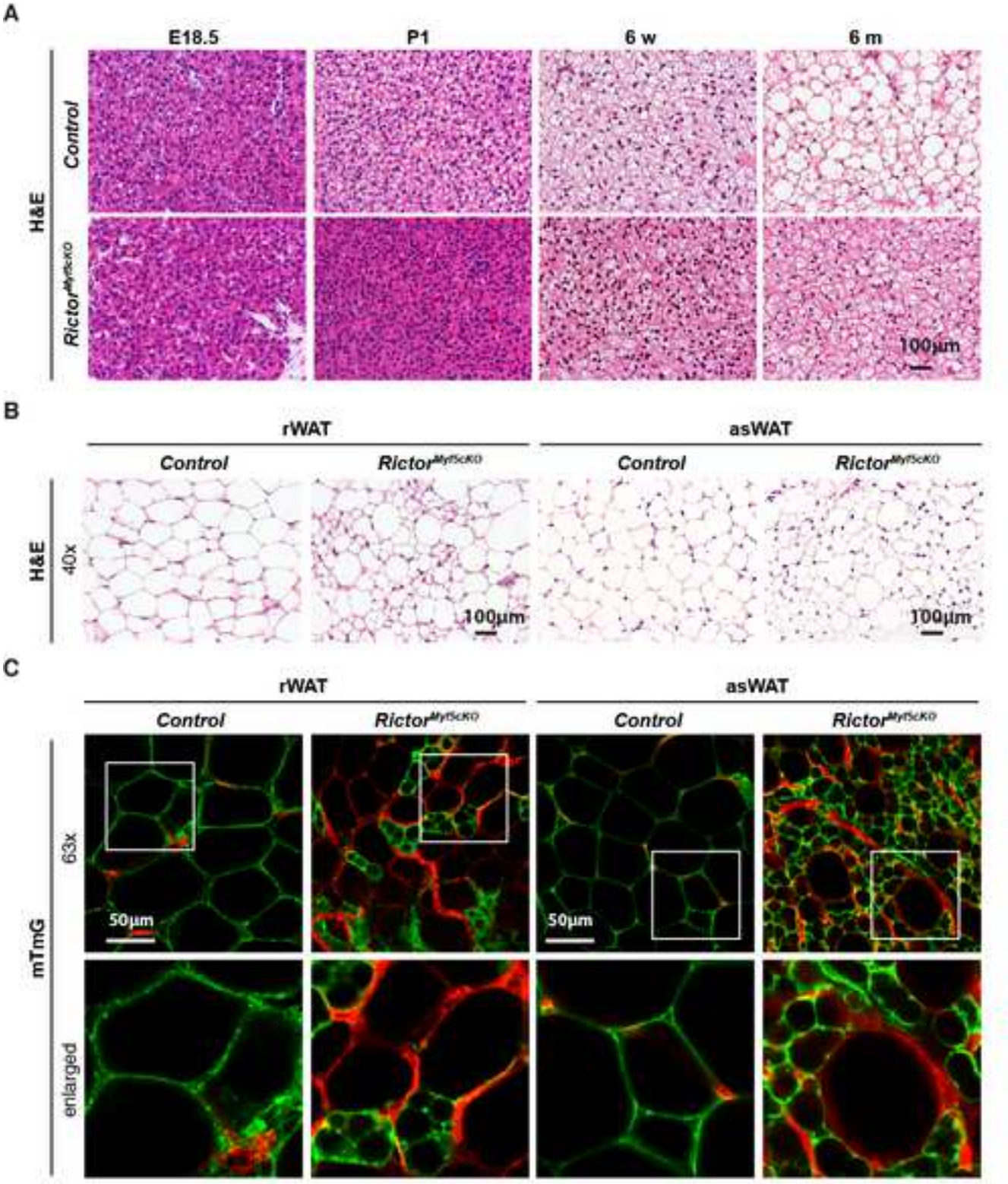

Figure 3

Click here to download high resolution image

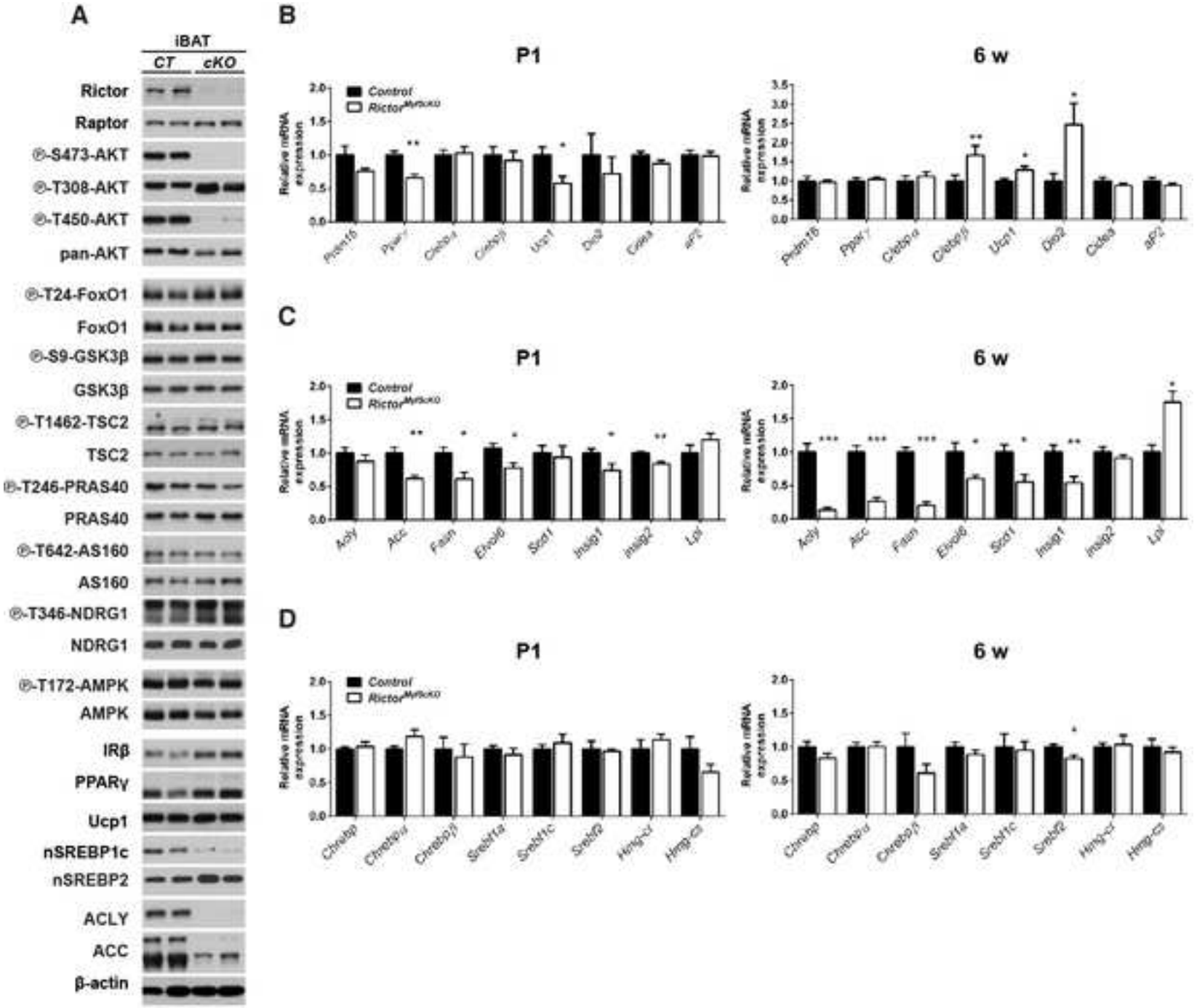

Figure 4

Click here to download high resolution image

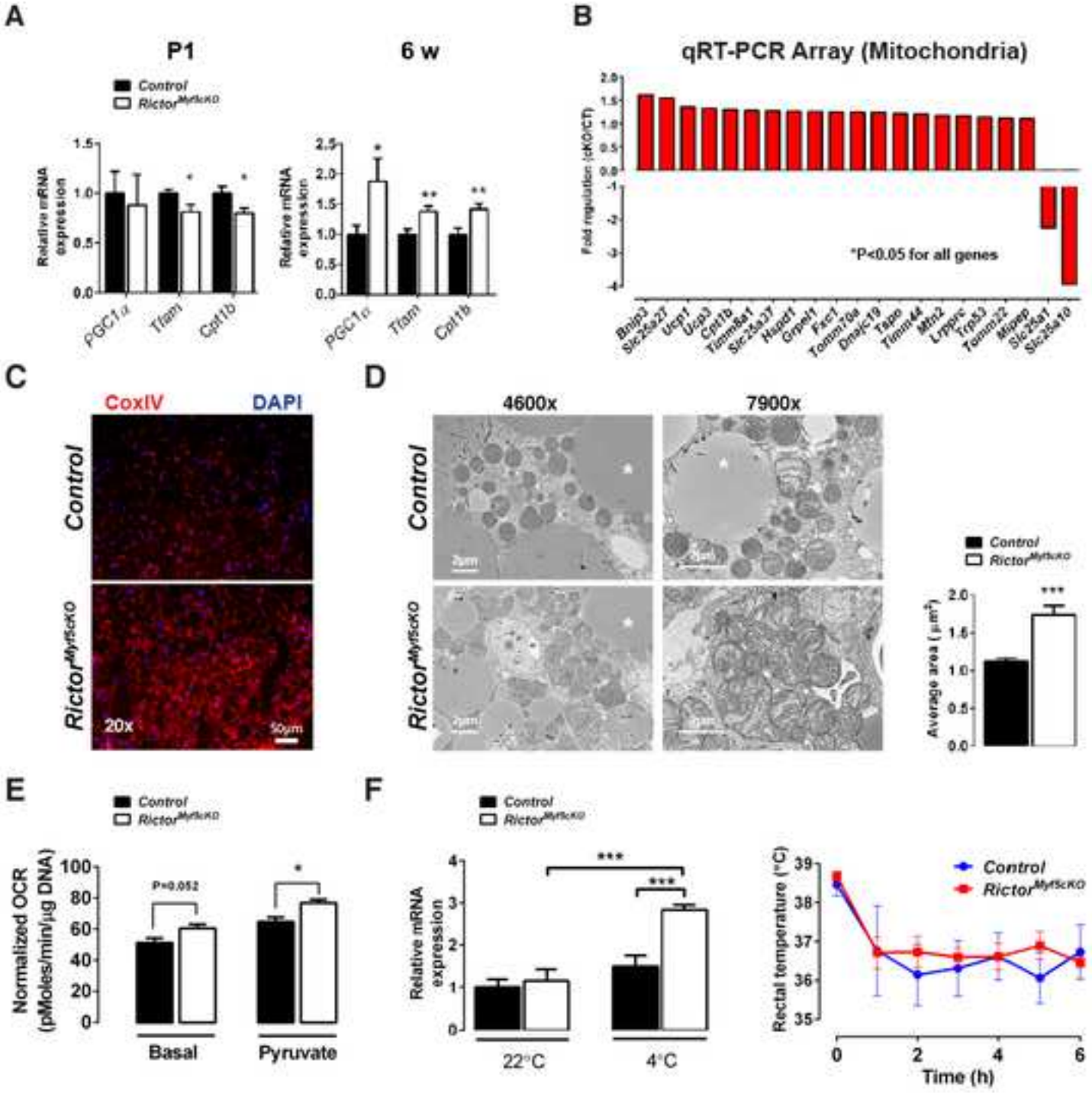

Figure 5
Click here to download high resolution image

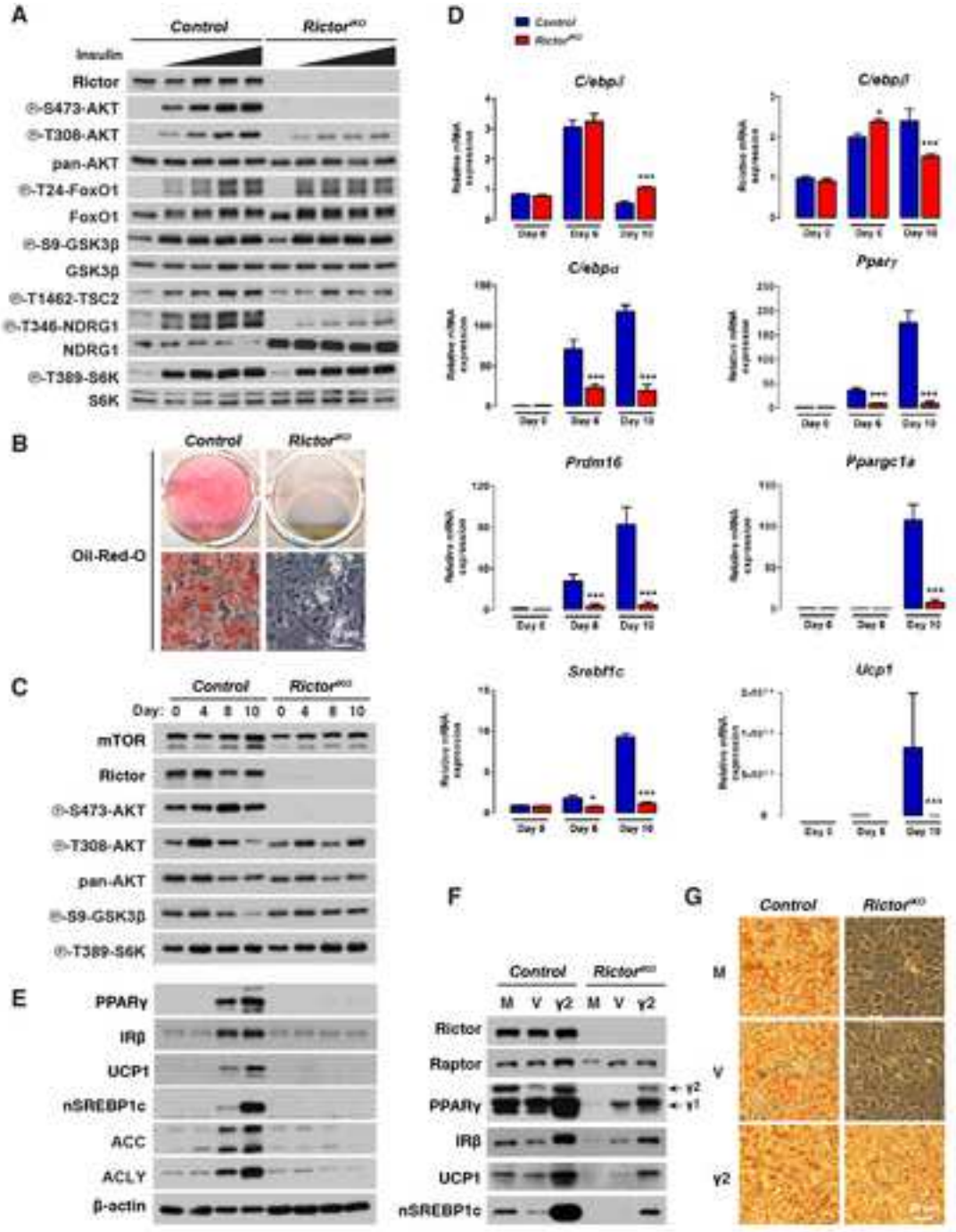

Figure 6
Click here to download high resolution image

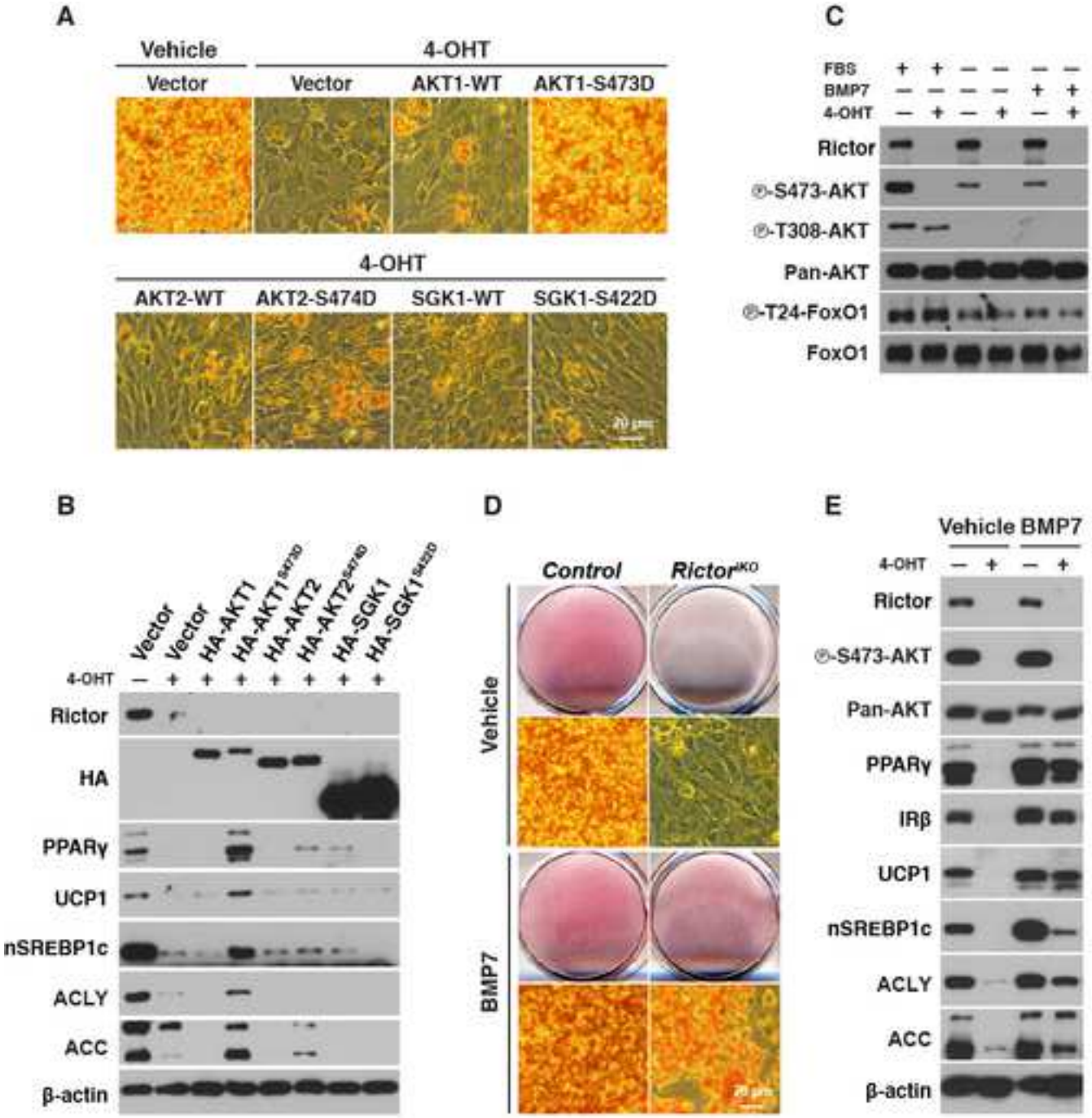

Figure 7

Click here to download high resolution image

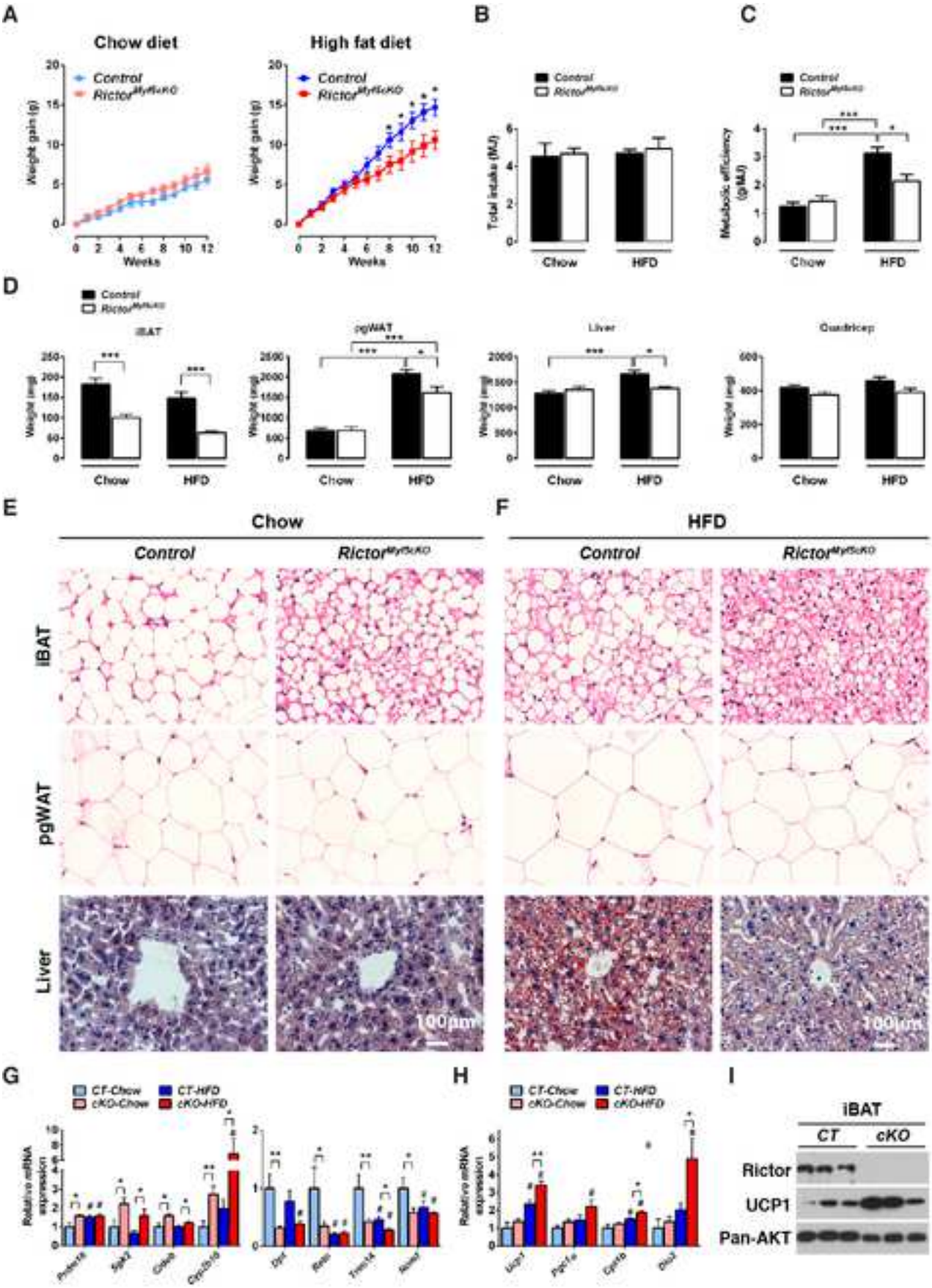

Supplemental Information

Rictor/mTORC2 Loss in the *Myf5*-lineage Reprograms Brown Fat Metabolism and Protects Mice against Obesity and Metabolic Disease

Chien-Min Hung, Camila Martinez Calejman, Juan Sanchez-Gurmaches, Huawei Li, Clary B. Clish, Simone Hettmer, Amy J. Wagers, and David A. Guertin

Inventory of Supplemental Information

Supplemental Information

Rictor/mTORC2 Loss in the *Myf5*-lineage Reprograms Brown Fat Metabolism and Protects Mice against Obesity and Metabolic Disease

Chien-Min Hung, Camila Martinez Calejman, Juan Sanchez-Gurmaches, Huawei Li, Clary B. Clish, Simone Hettmer, Amy J. Wagers, and David A. Guertin

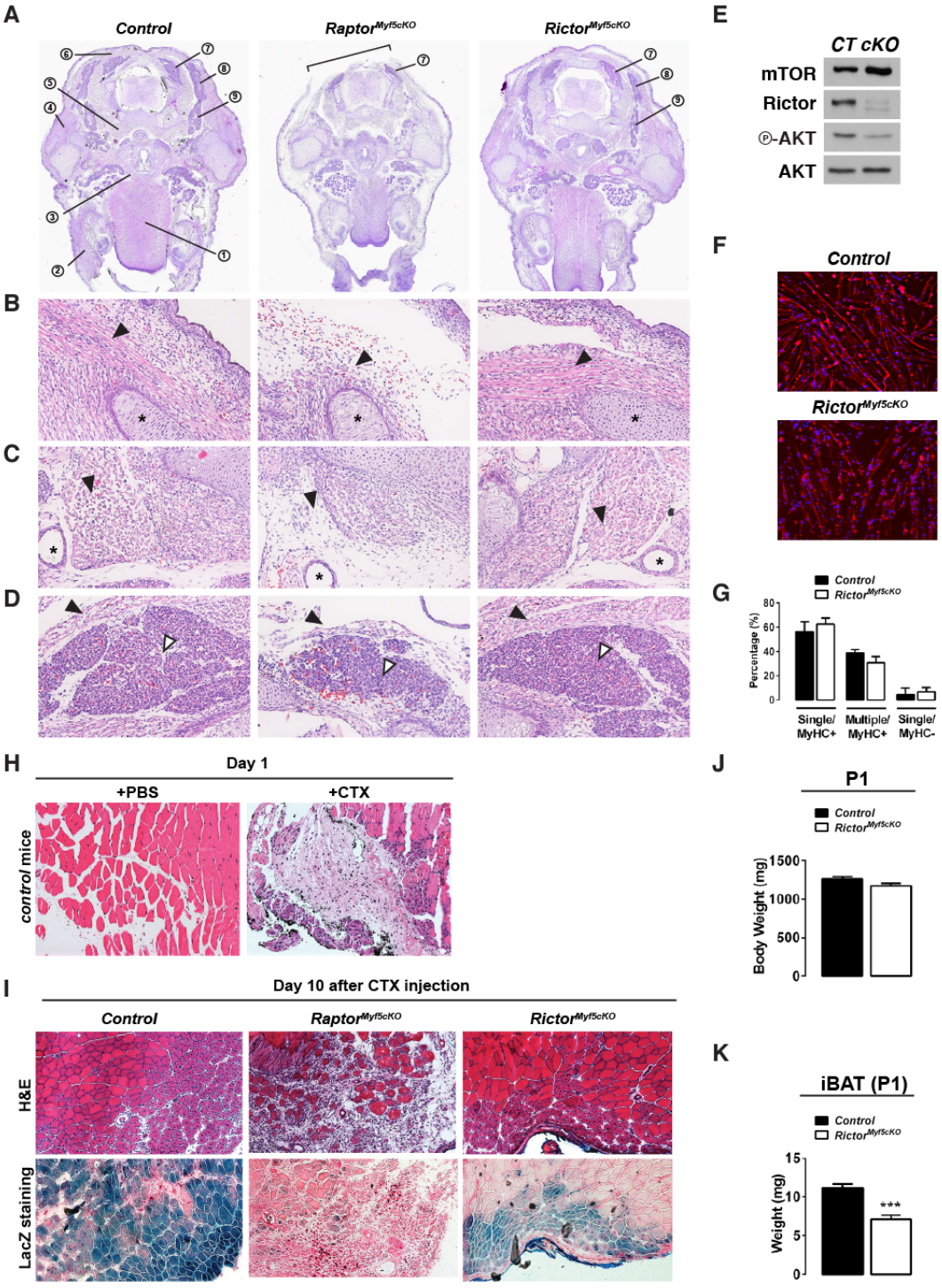

Figure S1, Related to Figure 1

(A) Transverse sections of E16.5 embryos. Tongue (1), masseter (2), sternohyoid and hyoglossus (3), supraspinatus (4), prevertebral (5), and trapezius muscles (7), and cervical BAT (7), interscapular BAT (8), and subscapular BAT precursors (9) are indicated. Bracket

marks region of hind neck fragility. **(B)** Enlarged image of supraspinatus muscle (arrowhead). Ossifying cartilage of the scapula marked with (*). **(C)** Enlarged image of prevertebral muscles of the neck (arrowhead). Carotid artery marked with (*). **(D)** Enlarged image of trapezius muscle (closed arrowhead) and cervical BAT precursors (open arrowhead). **(E)** Western blots of satellite cell lysates from control (*CT*) and *Rictor*^{Myf5cKO} conditional knockout (*cKO*) mice. **(F)** Differentiated satellite cells stained with myosin heavy chain antibody. **(G)** Quantification of nuclei number in individual differentiated satellite cells. **(H)** H&E images of tibialis anterior (TA) muscle 1 day after PBS or cardiotoxin injection in control mice (see also supplementary methods). **(I)** Mice deleted for *Raptor* or *Rictor* specifically in satellite cells with *Pax7*-CreER were subjected to an acute cardiotoxin injury assay. Mice also carried the *Rosa26-LacZ* reporter to follow the deleted cells. H&E images and corresponding images for LacZ staining of TA muscle 10 days after cardiotoxin injection. Regenerated muscle cells in the control and *Rictor* KO are indicated by the centrally localized nuclei in H&E stained sections. No regenerated cells are detectable in the *Raptor* KO. **(J-K)** Total body weight (J) and average iBAT weight (K) at postnatal day 1 (n=6; bars represent mean ± SEM; t-test; ***$p<0.001$).

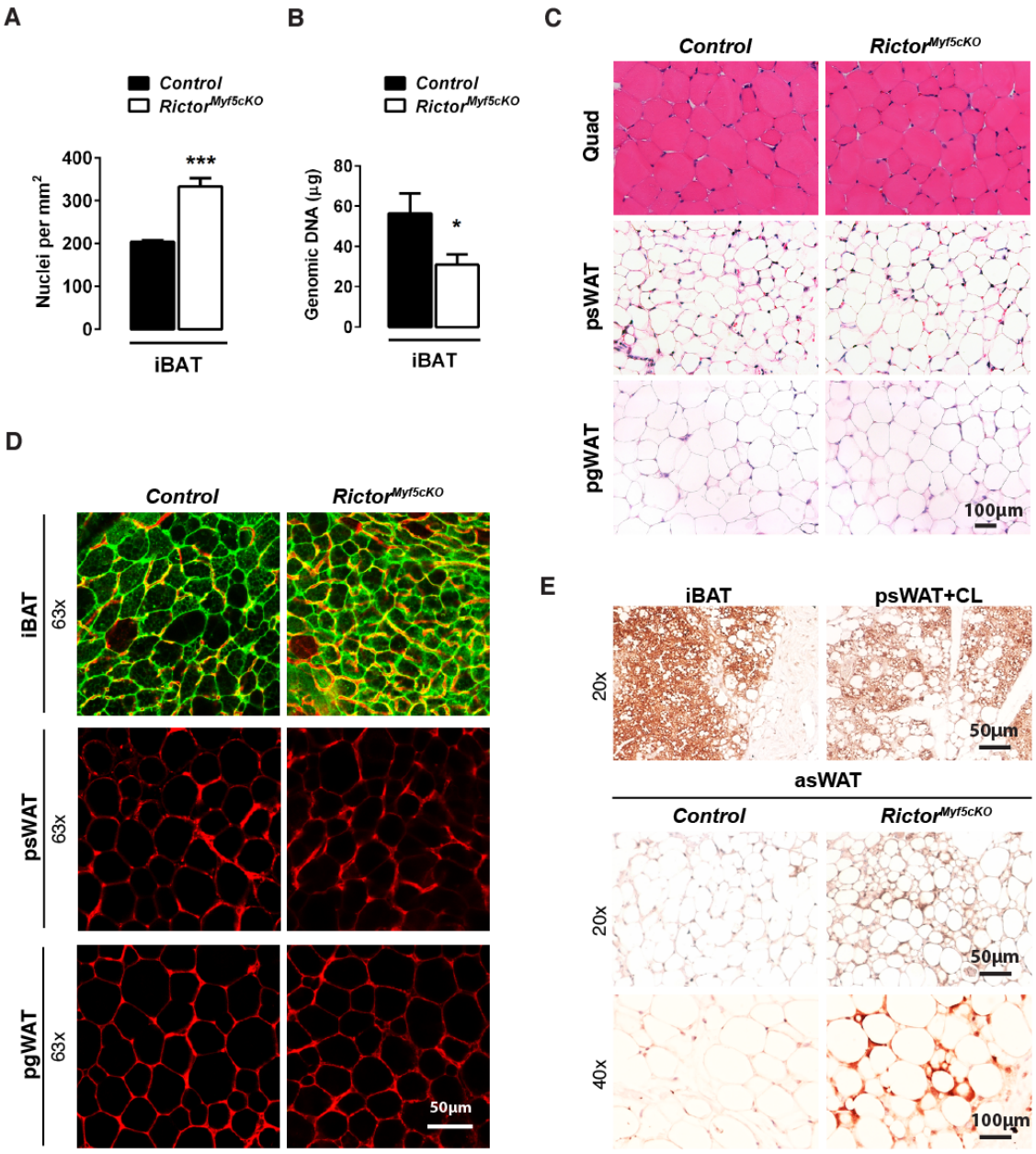

Figure S2, related to Figure 2.

(A) Nuclei density per mm^2 of iBAT (6-wks) (n=4; bars represent mean ± SEM; t-test; ***p<0.001). **(B)** Qunatification of genomic DNA from iBAT (6-wks) (n=8; bars represent mean ± SEM; t-test; *p<0.05). **(C)** H&E stains (40x) of the quadricep (Quad) muscle and posterior subcutaneous (psWAT) and perigonadal (pgWAT) white adipose tissue (6-wks). **(D)** Representative images of mTFP and mGFP labeled iBAT, psWAT and pgWAT adipocytes. Note adipocytes are homogenously mGFP$^+$ and smaller in the iBAT consistent with homogeneous *Rictor* loss in this tissue. **(E)** *Top*—UCP1 immunohistochemistry stains of iBAT and CL-316243 treated psWAT (20x). *Botton*—asWAT (20x and 40x) from control and *Rictor^{Myf5cKO}* mice.

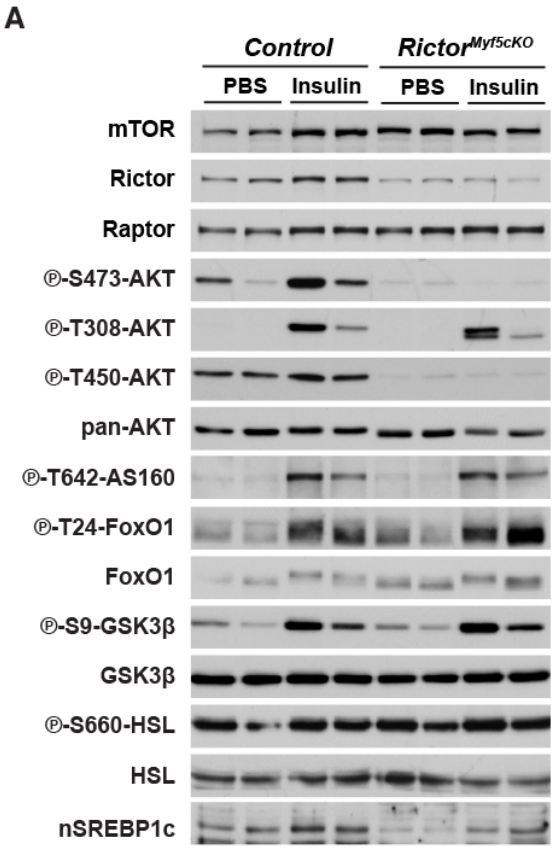

Figure S3, related to Figure 3.

(A) Western blots of the indicated total and phospho-proteins using lystates prepared from the iBAT of 8-week-old mice. Overnight fasted mice were *i.p*. injected with PBS or 150U/Kg insulin and tissues were collected 15 minutes post injection.

A

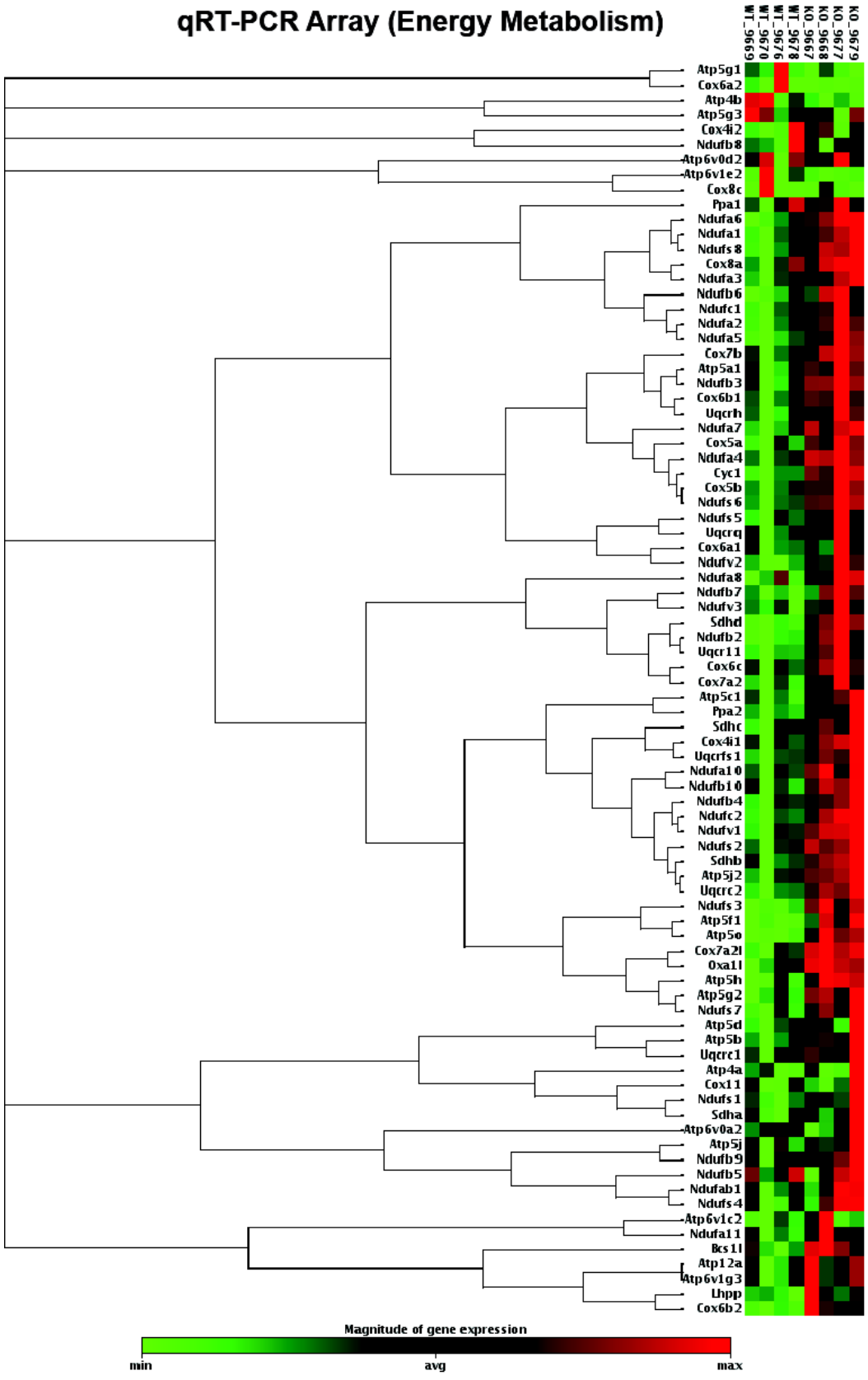
qRT-PCR Array (Energy Metabolism)
WT_9669
WT_9670
WT_9676
WT_9678
KO_9667
KO_9668
KO_9677
KO_9679
Atp5g1
Cox6a2
Atp4b
Atp5g3
Cox4i2
Ndufb8
Atp6v0d2
Atp6v1e2
Cox8c
Ppa1
Ndufa6
Ndufa1
Ndufs8
Cox8a
Ndufa3
Ndufb6
Ndufc1
Ndufa2
Ndufa5
Cox7b
Atp5a1
Ndufb3
Cox6b1
Uqcrh
Ndufa7
Cox5a
Ndufa4
Cyc1
Cox5b
Ndufs6
Ndufs5
Uqcrq
Cox6a1
Ndufv2
Ndufa8
Ndufb7
Ndufv3
Sdhd
Ndufb2
Uqcr11
Cox6c
Cox7a2
Atp5c1
Ppa2
Sdhc
Cox4i1
Uqcrfs1
Ndufa10
Ndufb10
Ndufb4
Ndufc2
Ndufv1
Ndufs2
Sdhb
Atp5j2
Uqcrc2
Ndufs3
Atp5f1
Atp5o
Cox7a2l
Oxa1l
Atp5h
Atp5g2
Ndufs7
Atp5d
Atp5b
Uqcrc1
Atp4a
Cox11
Ndufs1
Sdha
Atp6v0a2
Atp5j
Ndufb9
Ndufb5
Ndufab1
Ndufs4
Atp6v1c2
Ndufa11
Bcs1l
Atp12a
Atp6v1g3
Lhpp
Cox6b2
Magnitude of gene expression
min
avg
max

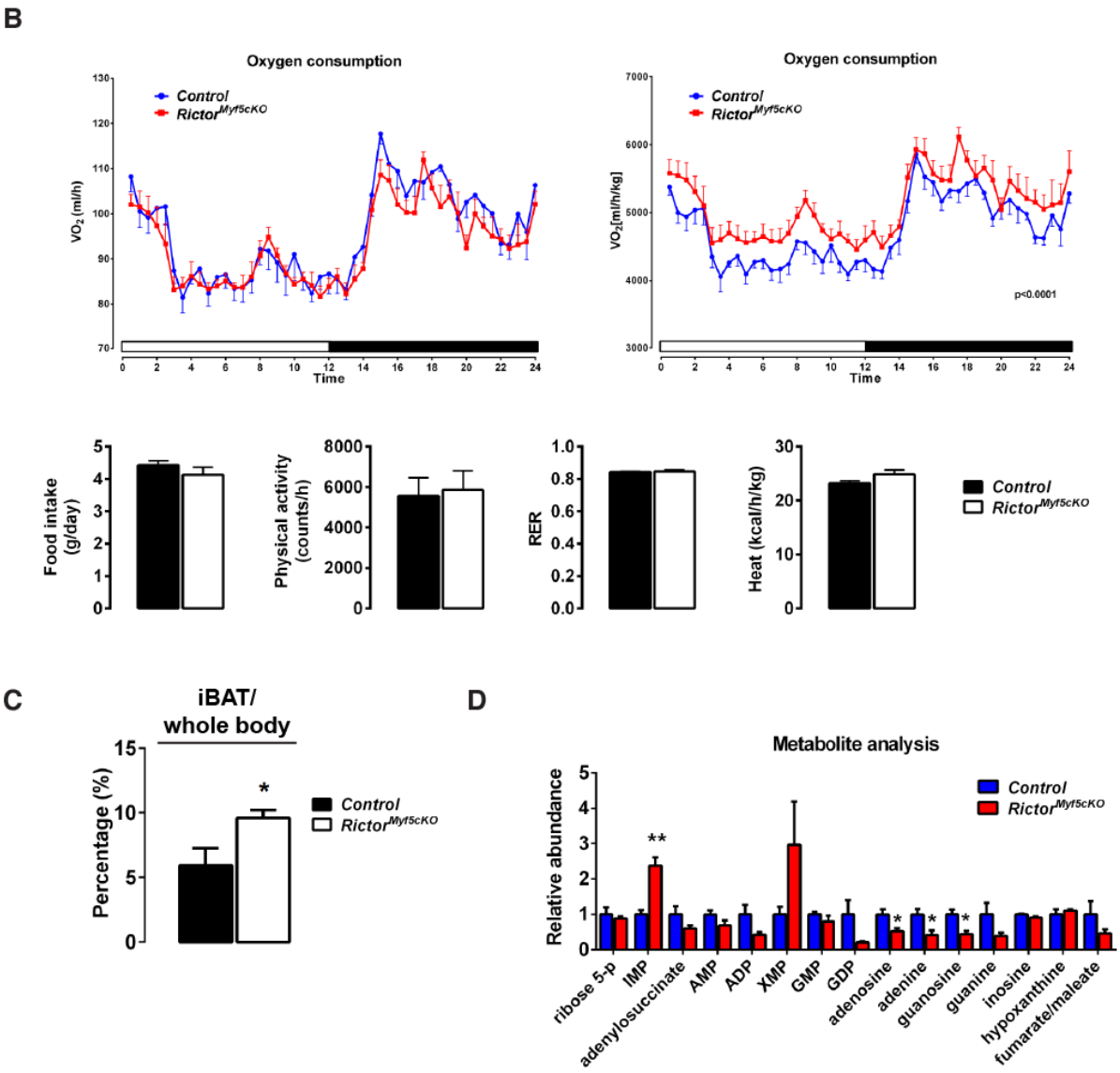

Figure S4, related to Figure 4.

(A) Clustering heat map for mitochondrial genes involved in energy metabolism qRT-PCR array (n=4). **(B)** Metabolic cage analysis of 6wk-old mice under normal housing temperature (22°C): *Top Left*—whole body oxygen consumption; *Top right*—whole body oxygen consumption normalized to body weight; *Botton*—food intake, physical activity, respiratory exchange ratio (RER) and energy expenditure. (n=6) **(C)** Glucose uptake by ^{18}FDG PET-CT (n=6; bars represent mean ± SEM; t-test; *p<0.05). **(D)** Metabolite profiling was performed on 6-week control and *Rictor^{Myf5cKO}* iBAT. Note the high levels of IMP, a deamination product of AMP. AMP is formed by the adenylate kinase reaction, which produces ATP (2ADP = AMP + ATP). During metabolic stress or following treatment with chemical uncouplers, AMP is deaminated to IMP to ensure ongoing adenylate kinase activity and ATP production in order to maintain energy balance (Balcke et al., 2011).

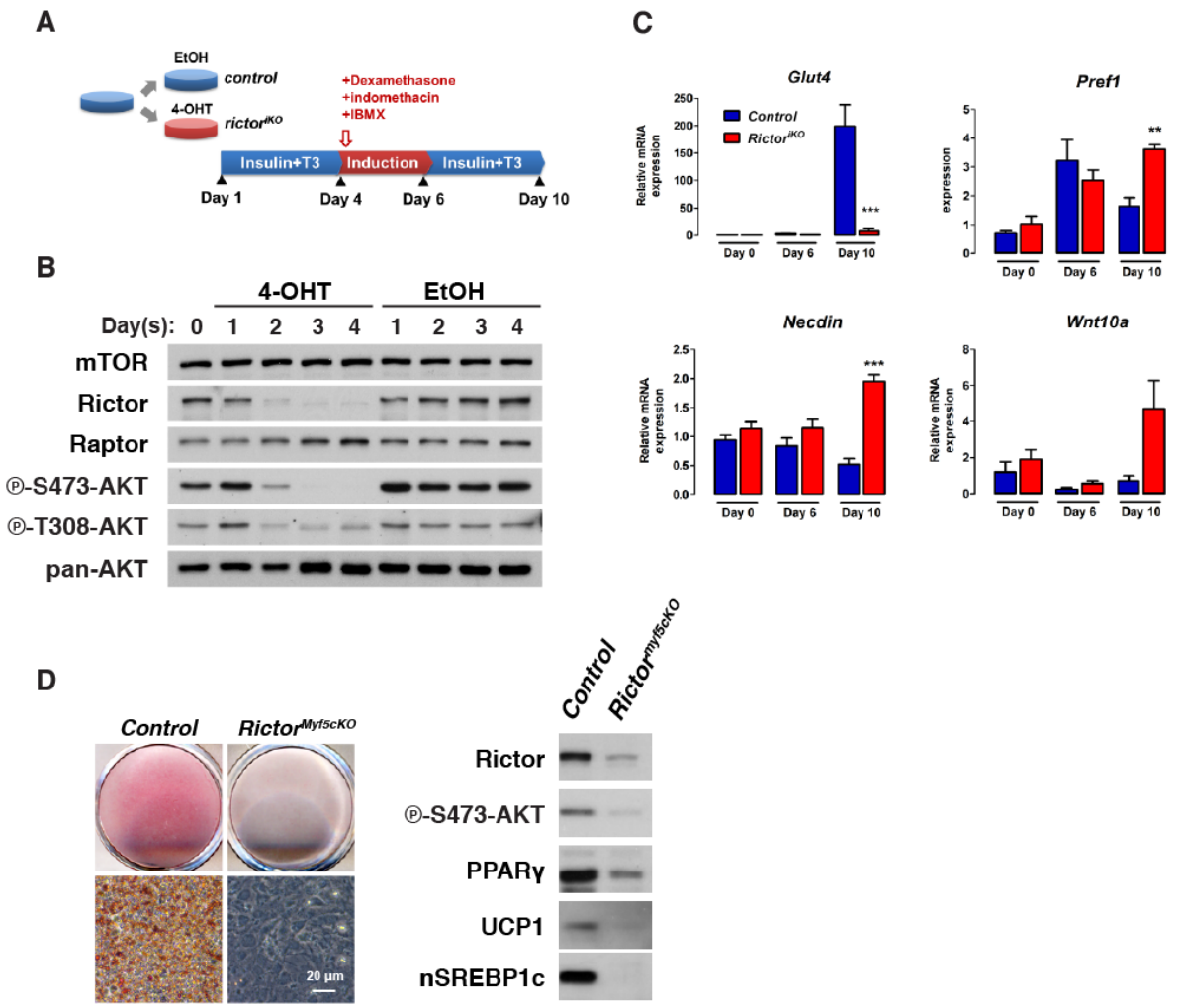

Figure S5, related to Figure 5.

(A) Inducible knockout differentiation protocol for comparing *Rictor*^{iKO} to isogenic control cells. Brown adipocyte precursors (bAPCs) were split from the same original dish into two dishes, one of which received vehicle (EtOH), the other 4-hydroxy-tamoxifem (4-OHT). After 3 days of treatment to induce deletion, cells were passed one time and then differentiated according to a standard 10-day brown adipocyte induction protocol (described in Experimental Procedures). **(B)** Western immunoblots showing time course following induced *Rictor* deletion in bAPCs with 4-OHT compared to vehicle (EtOH) treated isogenic controls. **(C)** qRT-PCR of mRNA levels for the indicated differentiation-related genes (n=3; bars represent mean ± SEM; t-test; *p<0.05, ***p<0.001). **(D)** *Left*—Oil Red O staining of control and *Rictor*^{Myf5cKO} bAPCs after differentiation. *Right*—Western immunoblots showing indicated differentiation markers.

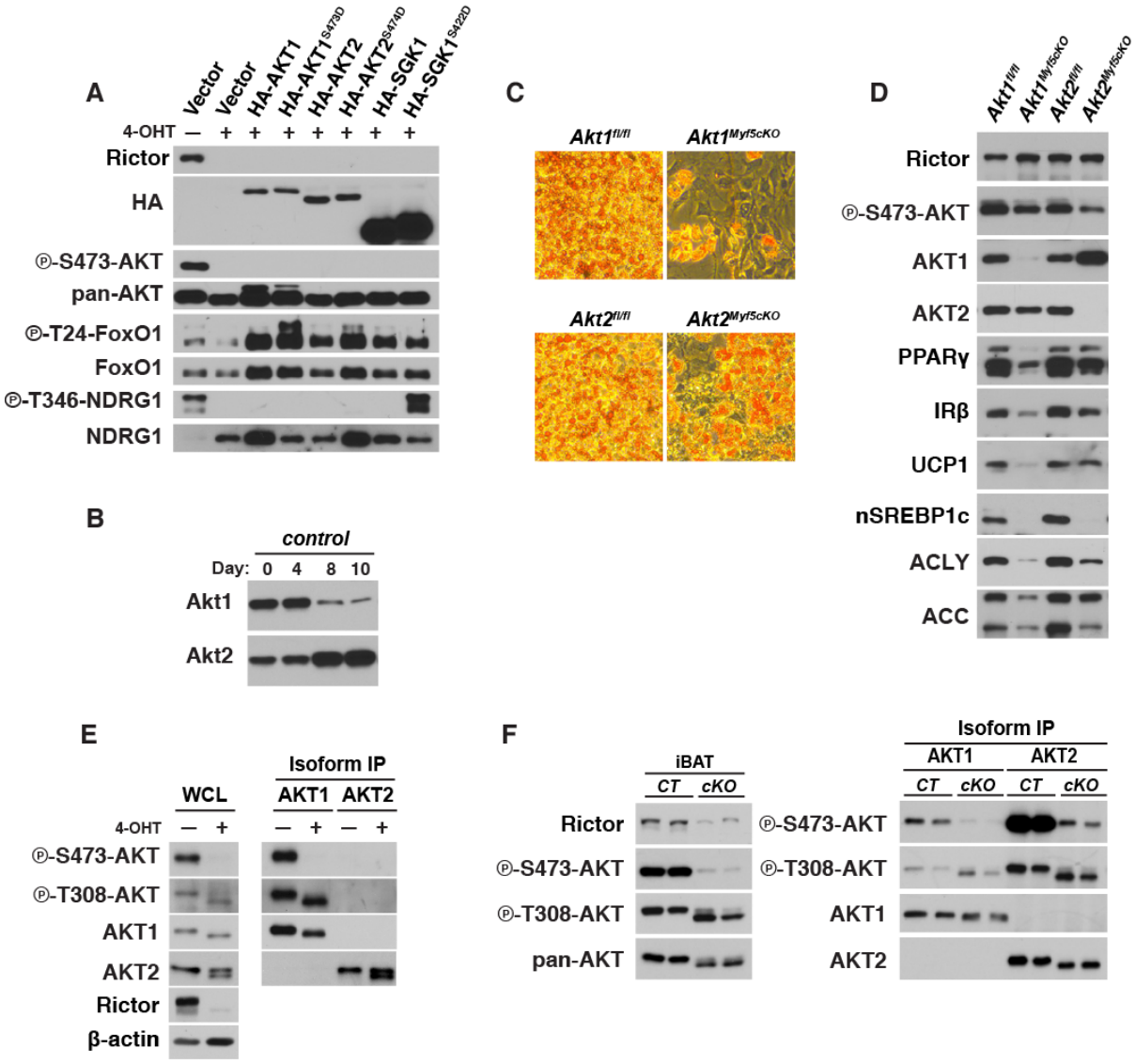

Figure S6, related to Figure 6.

(A) Western immunoblots of undifferentiated control and *Rictor*^{iKO} bAPCs stably expressing the indicated recombinant constructs. Cells were treated with fresh culture media before harvesting. **(B)** Western immunoblots of AKT1 and AKT2 protein expression at the indicated days during differentiation of wild type bAPCs. **(C)** Oil Red O staining of differentiated *Akt1* and *Akt2* conditional knockout and control bAPCs. The knockout cells were generated from *Myf5-cre;Akt1*$^{fl/fl}$ or *Myf5-cre;Akt2*$^{fl/fl}$ mice and the control cells are from their Cre-negative littermates. **(D)** Western immunoblots of lysates prepared from differentiated cells in (C). **(E)** Western immunoblots of lysates generated from AKT isoform-specific immunoprecipitation experiments using control or *Rictor*^{iKO} undifferentiated bAPCs. Immunoblots of the whole cell lystates (WCL) are shown to the left. **(F)** Western immunoblots of lysates generated from AKT isoform-specific immunoprecipitation experiments using iBAT dissected from 6-week-old control and *Rictor*^{Myf5cKO} mice.

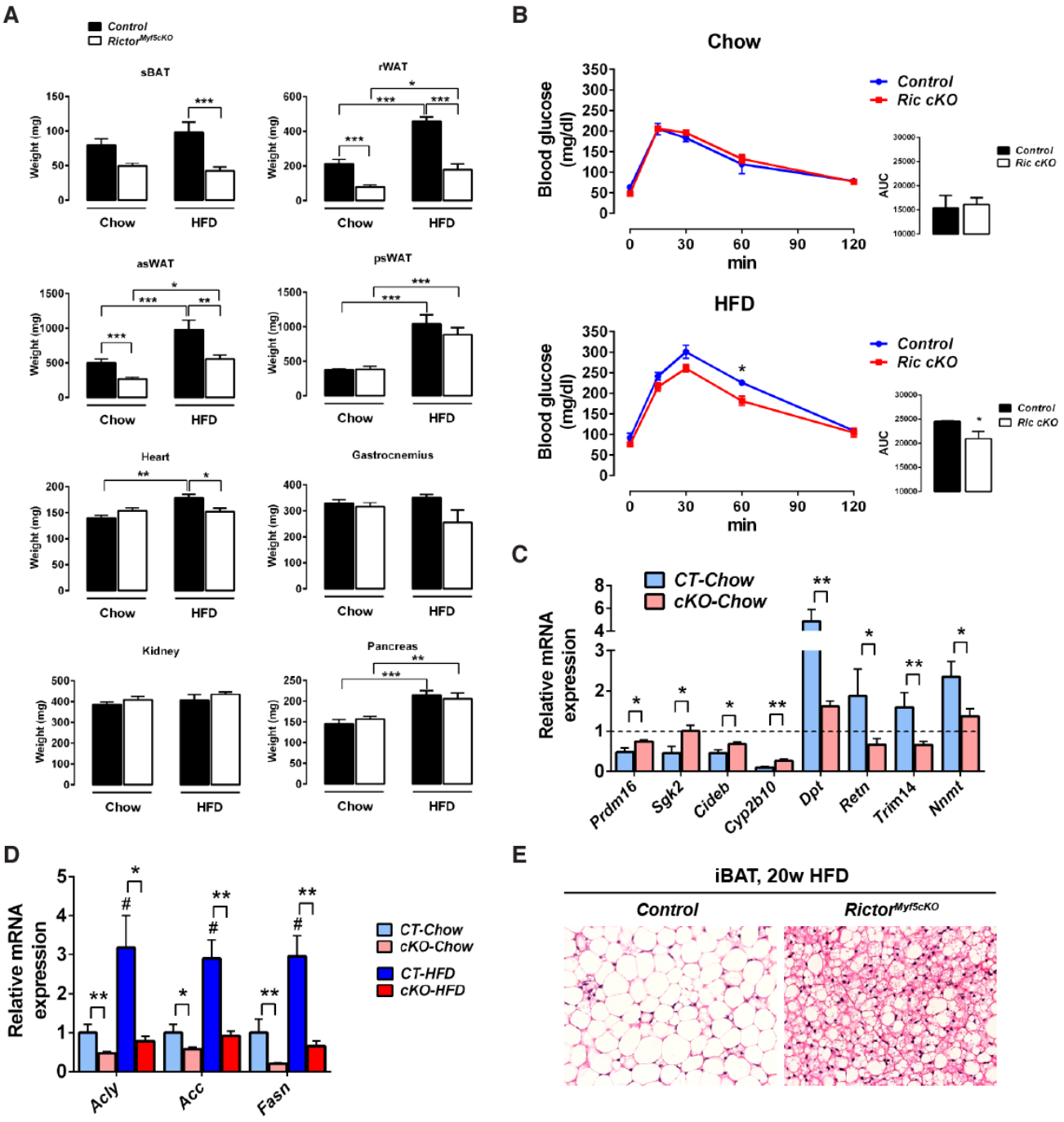

Figure S7, related to Figure 7.

(A) Mass (mg) of the indicated tissues collected from control and *Rictor*^{Myf5cKO} mice living at thermoneutrality (30°C) following 12-weeks of eating chow or HFD. (n=8 for control and n=12 for KO in chow; n=10 for both genotypes in HFD; bars represent mean ± SEM; two-way ANOVA; *p<0.05, ***p<0.001) **(B)** Glucose tolerance test of control and *Rictor*^{Myf5cKO} mice on chow (top) or HFD (bottom) living at thermoneutrality. The test was performed

during the 11th week of the 12-week experiment. **(C)** qRT-PCR of the indicated brown and white fat genes in iBAT from control and *Rictor*^{Myf5cKO} mice eating chow diet and living at thermoneutrality (n=8 for control and n=12 for KO in chow; bars represent mean ± SEM; two-way ANOVA; *p<0.05, **p<0.01, ***p<0.001). The expression level of each gene is normalized to the corresponding gene level in iBAT from age-matched control mice eating chow but living at the standard housing temperature (22°C). **(D)** qRT-PCR of the indicated lipogenesis genes in iBAT from chow or HFD mice (n=8 for control and n=12 for KO in chow; n=10 for both genotypes in HFD; bars represent mean ± SEM; two-way *ANOVA*; *p<0.05, **p<0.01, ***p<0.001; # indicates significant difference over the control chow group). **(E)** Representative H&E images (n=4) of control and KO mice fed with HFD at thermoneutrality for 20 weeks.

Supplemental Experimental Procedures

Embryo analysis

Timed matings were performed and embryos were dissected at the indicated days. Embryos were fixed overnight in paraformaldehyde, paraffin embedded, and processed for histological analysis according to conventional methods.

Mice

Mice were kept on a daily 12 h light/dark cycle and fed a normal chow diet (Prolab® Isopro® RMH 3000) from LabDiet ad libitum at 22°C (except thermoneutrality studies). All animal experiments were approved by the University of Massachusetts Medical school animal care and use committee.

Satellite cells isolation and in vitro differentiation

Limb muscle including triceps surae (TS), tibialis anterior (TA), quadriceps and triceps were dissected and minced from 6 to 8-wks mice. Isolated interstitial and myofiber-associated cells were passed through 70μm nylon mesh and centrifuged at 1200 rpm. Red blood cells were removed from preparations by incubation with RBC lysis buffer (0.15 M ammonium chloride, 0.01 M potassium bicarbonate) on ice for 3 minutes. Antibody staining was performed for 20 min on ice in Hank's balanced salt solution supplemented with 2% FCS and 2 mM EDTA. After staining cells were filtered through a 35-μm cell-strainer capped tube to ensure single cell suspension. Sorting was performed immediately after filtration using a FACS Aria II cell sorter equipped with FASCDiva software. Cells were initially selected by size and shape and only live (PI-, calcein blue+) singlets were gated for further analysis of surface markers. Finally an enriched pool of cells (Sca-1-, Mac1-, Ter119-, CD45-, CXCR4+ and β1 intergrin+) were purified and re-sorted with the same scheme described above to ensure the purity. Double sorted satellite cells were plated at $4x10^3$ cells/well in collagen/laminin coated 96-well plates. Cells were maintained in growth media (20% horse serum in F10 media, Invitrogen) and feed with 5ng bovine FGF daily for 5 days. For inducing muscle fiber formation, cells were first transferred into matrigel (BD Biosence)-coated chamber slides and grown in growth media with bFGF. 2~3

days later, cells were exposed to differentiation media (2% horse serum in F10 without bFGF). After 2 to 4 days myofiber can be observed and fixed with 4% paraformaldehyde. Myosin heavy chains and DAPI staining were performed as described in immunofluorescence section.

Muscle regeneration after cardiotoxin injury

To induce *Rictor* deletion in vivo, *Pax7-CreER^{T2}* mice were i.p. injected with 200µg/g of tamoxifen (dissolved in ethanol first then diluted in corn oil to 10mg/mL) for consecutive 4 days. One day later the mice were anesthetized with 12mg/kg xylazine and 60mg/kg ketamine and 30µL cardiotoxin (10µmol/L from *Naja nigricollis,* Calbiochem) was directly injected into tibialis anterior muscle. 30µL PBS was given in contralateral TA muscle as control. 1 day and 10 days post injury, TA muscle was removed and muscle regeneration was examined by H&E staining and LacZ staining.

LacZ staining

Adipose tissue depots were fixed in 2% paraformaldehyde, 0.2% glutaraldehyde in PBS for 30 min at room temperature. The tissues were then washed 3 times for 15 min in wash buffer (PBS carrying 2 mM MgCl2 and 0.02% Igepal® CA-630). Staining was perform in wash buffer containing X-gal (1mg/mL), potassium ferricyanide (5 mM) and potassium ferrocyanide (5 mM) at room temperature for at least 16 h. Next, tissues were further fixed in fixing solution for at least 12 h at room temperature, transferred to ethanol for dehydratation, then sectioned at 5 µm thicknesses. Sections were counter-stained with nuclear fast red dehydrated and mounted using CitosealTM 60 (Thermo Scientific). Lean tissues were snap frozen in isopentane-liquid nitrogen in OCT. Sections (10 µm) were stained overnight (X-gal (1mg/mL), potassium ferricyanide (5 mM) and potassium ferrocyanide (5 mM), MgCl2 (2 mM) in PBS at 37°C and counter-stained with nuclear fast red, dehydrated and mounted.

Tissue harvest and histology

Adipose tissue depots notations are described in (Walden et al., 2011). Each tissue was carefully dissected to avoid contamination from surrounding tissue. Samples for RNA were

first immersed in RNAlater (Invitrogen) and stored at -80°C; otherwise, they were frozen down immediately in liquid nitrogen. For histology, tissue pieces were fixed by 10% formalin. Embedding, sectioning and Hematoxylin & Eosin (HE) staining was done by the UMass Morphology Core.

Immunohistochemistry

Adipose tiss sections were subjected to UCP1 IHC according to (Cohen et al., 2014). Briefly, fat sections were hydrated and antigen retrieval was done by incubating the sections in citrate buffer at 90-95°C water for 20 min. After blocking, primary antibody (anti-Ucp1 antibody, Abcam #ab10983) was applied overnight at 4°C. Next day, SuperPicture 3rd Gen IHC Detection Kit (Novex) was used for detection.

Whole-mount confocal microscopy

Indicated brown and white adipose tissues were dissected from 6 week-old mice and were mounted with Fluoromount-G (Southern Biotech) as described in (Berry and Rodeheffer, 2013). Mounted samples were imaged on a LSM 5 Pascal (Zeiss) point scanner confocal system. 40x objective was used with oil immersion. Background fluorescence was offset by using wild-type tissues (no *mT/mG* allele). GFP was excited at 488 nm and detected from 515 to 565 nm and iBAT form *Myf5-cre;Rosa26mT/mG* mice was used as positive control for GFP signal. TdTomato was excited at 543 nm and detected from 575 to 640 nm and pgWAT from mT/mG mice (without Cre-driver) was used as positive control for TdTomato.

Nuclei number and cell size quantification

ImageJ was used to quantify nuclei number in iBAT and cell size (diameter) in rWAT and asWAT. For each individual sample, 4 to 6 images were taken and analyzed. Nuclei density was presented as nuclei number per mm^2.

Genomic DNA quantification

Total genomic DNA was extracted and purified by using DNeasy Blood & Tissue kit (Qiagen) according to manufacturer's instruction. Isolated genomic DNA was quantified by NanoDrop 2000 (Thermo Scientific) spectrophotometer.

Immunofluorescence

Frozen section of interscapular brown adipose tissues were thawed and then fixed with methanol for 15 min at room temperature. The fixed sections were washed with 1mL PBS twice and then were permeabilized and blocked with PBSAT buffer (PBS with 1% BSA and 0.5% Triton X-100) for 15 min twice. Primary antibody against mitochondria Cox IV (1:100 dilution, CST #4850) was added to sections for overnight incubation. Slides were washed three times with 1mL PBSAT and incubated with secondary antibody conjugated with Alexa-568 or Alexa-647 (1:1000 dilution, Invitrogen) for 4 hours. Intensive wash was applied to remove unstained antibodies. DAPI was used to stain nuclei for 5 min and washed away by PBS immediately. The slides were embedded with 5μL mounting media (Prolong Gold, Invitrogen).

Glucose uptake

6-week old mice (n=5 per each genotype) were i.p. injected with ^{18}F-FDG, 364-483 uCi in100 ul saline, and 30 min later the PET imaging was performed in anesthetized animals (1.2-2% isoflurane carried in oxygen) immobilized on a Minerve bed (Bioscan). Immediately after PET acquisition, each mouse was transferred to the NanoSPECT/CT (Bioscan), for the CT acquisition. The PET images were reconstructed without photon attenuation correction using the PETView program (Philips) with the fully 3D iterative reconstruction algorithm, giving a pixel size of 1 mm. The CT acquisition was performed at standard frame resolution, 45 kVp tube voltage and 500 ms of exposure time. The CT reconstruction was accomplished using In-VivoScope 1.37 software (Bioscan). The PET image DICOM files were transferred to the NanoSPECT/CT reconstruction workstation to provide the PET/CT fusion images. Volume-of-Interest (VOI) analysis of the PET acquisitions was accomplished with the InVivo- Scope 1.37 software.

Transmission electron microscopy

iBATs (n=3 for each group) were dissected from 5 week-old mice and subjected to electron microscopy study done by Core Electron Microscopy Facility, UMass medical school.

Metabolite profiling

Brown fat samples were homogenized in four volumes of water using a TissueLyser II (Qiagen) and profiles of polar metabolites were obtained using LC-MS. The polar metabolite profiling methods were developed using reference standards of each metabolite to determine chromatographic retention times and MS multiple reaction monitoring transitions, declustering potentials and collision energies. The LC-MS methods have been recently described (Townsend et al., 2013). Briefly, negative ionization mode data were acquired using an ACQUITY UPLC (Waters) coupled to a 5500 QTRAP triple quadrupole mass spectrometer (AB SCIEX) running hydrophilic interaction chromatography (HILIC) method. A 30µL aliquot of each homogenate was extracted using 120 µL of 80% methanol (VWR) containing 0.05 ng/µL inosine-15N4, 0.05 ng/µL thymine-d4, and 0.1 ng/µL glycocholate-d4 as internal standards (Cambridge Isotope Laboratories). The samples were centrifuged (10 min, 9,000 x g, 4ºC) and the supernatants (10 µL) were injected directly onto a 150 x 2.0 mm Luna NH2 column (Phenomenex) that was eluted at a flow rate of 400 µL/min. Initial mobile phase conditions were 10% mobile phase A (20 mM ammonium acetate and 20 mM ammonium hydroxide (Sigma-Aldrich) in water (VWR)) and 90% mobile phase B (10 mM ammonium hydroxide in 75:25 v/v acetonitrile/methanol (VWR)) and the column was eluted using a 10 min linear gradient to 100% mobile phase A. The ion spray voltage was -4.5 kV and the source temperature was 500°C. Positive ionization mode data were acquired using an 1100 Series pump (Agilent) and an HTS PAL autosampler (Leap Technologies) coupled to a 4000 QTRAP triple quadrupole mass spectrometer (AB SCIEX). A 10µL aliquot of each homogenate was extracted using nine volumes of 74.9:24.9:0.2 (v/v/v) acetonitrile/methanol/formic acid containing stable isotope-labeled internal standards (0.2 ng/µL valine-d8, Isotec; and 0.2 ng/µL phenylalanine-d8 (Cambridge Isotope Laboratories)). Samples were centrifuged (10 min, 9,000 x g, 4ºC) and supernatants (10 µL) were injected onto a 150 x 2.1 mm Atlantis HILIC column (Waters).

The column was eluted isocratically at a flow rate of 250 µL/min with 5% mobile phase A (10 mM ammonium formate and 0.1% formic acid in water) for 1 minute followed by a linear gradient to 40% mobile phase B (acetonitrile with 0.1% formic acid) over 10 minutes. The ion spray voltage was 4.5 kV and the source temperature was 450°C. MultiQuant 1.2 software (AB SCIEX) was used for automated peak integration and metabolite peaks were manually reviewed for quality of integration and compared against a known standard to confirm identity.

Cold challenge

Mice were first fasted for 16 hours and transferred into a 4°C cold room without any food in the cage. Rectal temperature was measured by rectal probe (RET-3, ThermoWorks) hourly for 6 hours. Mice were sacrificed and tissues were collected at the end of experiment. Fasted mice kept at 22°C were used as control for qRT-PCR.

Cell culture and retrovirus production

All cells were cultured in DMEM (Invitrogen) supplemented with 10% FBS and penicillin/streptomycin at a 37°C. Primary brown preadipocytes (bBPAs) were isolated from P1 neonates of *Ubc-creER^{T2};Rictor$^{fl/fl}$* mice, *Myf5-cre;Rictor$^{fl/fl}$*,*Myf5-cre;Akt1$^{fl/fl}$*, *Myf5-cre;Akt2$^{fl/fl}$* mice and control littermates according to (Fasshauer et al., 2001) and were immortalized with pBabe-SV40 Large T antigen and selected by puromycin resistance. For recombinant AKT and SGK construct expression, retroviruses were made by cotransfecting pBabe-puro plasmid harboring different *Akt* or *Sgk* cDNAs with pCL-Ampho in HEK-293T cells. 24h and 48h after transfection the viral supernatant was harvested and applied to MEFs for 12h. Cells stably expressing each construct were obtained after puromycin selection.

Differentiation

To generate *Rictor^{iKO}* cells *ubc-creER^{T2};Rictor$^{fl/fl}$* bAPCs were treated with two doses of 1µM 4-OHT for 3 days. For brown preadipocyte differentiation, BPAs were seeded at 4x10^4 cells/ml and allowed to proliferate to confluence over 3 days in differentiation media (20nM insulin, 1nM T_3). On the 4th day, cells were induced to differentiate by adding

induction media (20nM insulin, 1nM T_3, 0.125mM indomethacin, 2μg/mL dexamethasone and 0.5mM 3-isobutyl-1-methylxanthine (IBMX)) for 2 days; the medium was then changed every two days with fresh differentiation media until day 10. Differentiated bAPCs were fixed with PBS-buffered formalin and stained with Oil-Red-O dye.

Western blots

Cells were lysed in a buffer containing 50mM Hepes, pH 7.4, 40mM NaCl, 2mM EDTA, 1.5mM $NaVO_4$, 50mM NaF, 10mM sodium pyrophosphate, 10mM sodium β-glycerophosphate and 1% Triton X-100 typically 1 hour after the cells were replenished with fresh culture medium. Tissues were homogenized using a TissueLyser (Qiagen) in the same lysis buffer but additionally supplemented with 0.1% SDS, 1% sodium deoxycholate. An equal amount of total protein was loaded into acrylamide/bis-acrylamide gels and transferred to PVDF membranes for detection with the indicated antibodies. Briefly, membranes were incubated with primary antibodies in 5% milk/PBST or 5% BSA/PBST overnight. HRP-conjugated secondary antibodies were given for 1h. Western blots were developed by enhanced chemiluminescence (PerkinElmer) and detected by X-ray films.

Immunoprecipitation

AKT1-specific antibody (CST# 2967) and AKT2-specific antibody-conjugated beads (CST#4090) were used to purify each isoform. 500ug Cell lysates or tissue lysates were incubated with 1ul of antibodies at 4°C overnight. For AKT1 purification, protein-antibody complex was precipitated by 2 hrs incubation with protein G sepharose beads (Invitrogen). Samples were then boiled in 2x SDS sample buffer.

***Ex vivo* oxygen consumption**

Freshly isolated brown adipose tissues were rinsed with KHB buffer (111nM NaCl, 4.7mM KCl, 2mM $MgSO_4$, 1.2mM Na_2HPO_4, 0.5mM carnitine and 2.5mM glucose) and then cut into small pieces (5~10mg). After 5 times of washing with KHB buffer, each piece was placed into the center of one single well in a XF24 islet capture microplate (Seahorse Bioscience #101122-100) and covered by a provided screen. 450ul KHB buffer was loaded in each well and tissue

metabolic rates were measured following program: 3 cycles for basal oxygen consumption rate (OCR) (2 min mix, 2 min wait, and 3 min measure), then injection of 50ul 100mM pyruvate, then followed by 3 cycles for pyruvate-stimulated OCR (3 min mix, 3 min wait, and 2 min measure). Each OCR value was obtained from five different pieces of a tissue and from 3 repeated measurements. The final OCR values were the average of five independent experiments and normalized to genomic DNA content.

Gene expression analysis

Total RNA was isolated from cells or tissues using Qiazol (Invitrogen) and an RNeasy kit (Invitrogen). Equal amounts of RNA were retro-transcribed to cDNA using a High capacity cDNA reverse transcription kit (#4368813, Applied Biosystems). Quantitative RT-PCR was performed in 10μL reactions using a StepOnePlus real-time PCR machine from Applied Biosystems using SYBR Green PCR master mix (#4309156, Applied Biosystems) according to manufacturer instructions. Standard and melting curves were run in every plate for every gene to ensure efficiency and specificity of the reaction. *Tbp* expression was used as a normalization gene in all conventional RT-PCR experiments. Primer information is listed in the table below. Quantitative RT-PCR arrays for mitochondria (PAMM-087) and mitochondria energy metabolism (PAMM-008) were purchased from Qiagen. Interscapular brown fat pads were removed from 6-wks mice *ad libitum* and Rictor protein deletion in *Myf5-re;Rictor*$^{fl/fl}$ samples was confirmed by western blots before analyzing expression. Data analysis was performed on web-based software provided by the manufacturer.

Primer sequences for quantitative RT-PCR analysis

Gene	Forward primer (5'-3')	Reverse primer (5'-3')
Tbp	GAAGCTGCGGTACAATTCCAG	CCCCTTGTACCCTTCACCAAT
Prdm16	GACATTCCAATCCCACCAGA	CACCTCTGTATCCGTCAGCA
Ppargc1α	CCCTGCCATTGTTAAGACC	TGCTGCTGTTCCTGTTTTC
Pparγ	TCAGCTCTGTGGACCTCTCC	ACCCTTGCATCCTTCACAAG
C/ebpα	CAAGCCCAGCAACGAGTACCG	GTCACTGGTCAACTCCAGCAC
C/ebpβ	TCGGGACTTGATGCAATCC	AAACATCAACAACCCCGC
C/ebpδ	GCTTTGTGGTTGCTGTTGAA	ATCGACTTCAGCGCCTACA

Ucp1	CTGCCAGGACAGTACCCAAG	TCAGCTGTTCAAAGCACACA
DiO2	TGCGCTGTGTCTGGAACAG	CTGGAATTGGGAGCATCTTCA
Lpl	GGCCAGATTCATCAACTGGAT	GCTCCAAGGCTGTACCCTAAG
aP2	GATGCCTTTGTGGGAACCT	CTGTCGTCTGCGGTGATTT
Cidea	ATCACAACTGGCCTGGTTACG	TACTACCCGGTGTCCATTTCT
Dpt	CTGCCGCTATAGCAAGAGGT	TGGCTTGGGTACTCTGTTGTC
Srebf1a	TAGTCCGAAGCCGGGTGGGCGCCGG	GATGTCGTTCAAAACCGCTGTGTGTC
Srebf1c	AAGCAAATCACTGAAGGACCTGG	AAAGACAAGCTACTCTGGGAG
Srebf2	GGATCCTCCCAAAGAAGGAG	TTCCTCAGAACGCCAGACTT
Chrebp	CACTCAGGGAATACACGCCTAC	ATCTTGGTCTTAGGGTCTTCAGG
Chrebpα	CGACACTCACCCACCTCTTC	TTGTTCAGCCGGATCTTGTC
Chrebpβ	TCTGCAGATCGCGTGGAG	CTTGTCCCGGCATAGCAAC
Acly	CTCACACGGAAGCTCCATAA	ACGCCCTCATAGACACCATC
Acc	GGAGATGTACGCTGACCGAGAA	ACCCGACGCATGGTTTTCA
Fasn	GCTGCGGAAACTTCAGGAAAT	AGAGACGTGTCACTCCTGGACTT
Elvol6	TCAGCAAAGCACCCGAAC	AGCGACCATGTCTTTGTAGGAG
Scd1	CCCTGCGGATCTTCCTTATC	TGTGTTTCTGAGAACTTGTGGTG
Insig1	TGTGGTTCTCCCAGGTGACT	TAGCCACCATCTTCTCCTCC
Insig2	TGAAGCAGACCAATGTTTCAA	GGTGAACTGGGGGTCTCC
Tfam	GTCCATAGGCACCGTATTGC	CCCATGCTGGAAAAACACTT
Cpt1b	GGGCACCTCTGGGAGTTTGT	TTGGCTCACCCACACAGTGT
Necdin	CACTTCCTCTGCTGGTCTCC	ATCGCTGTCCTGCATCTCAC
Pref1	AGTACGAATGCTCCTGCACAC	CTGGCCCTCATCATCCAC
Wnt10a	CACCCGGCCATACTTCCT	CACTTACGCCGCATGTTCT

*Primer sequences for the brown and white fat marker genes *Sgk2, Cideb, Cyp2b10, Retn, Trim14* and *Nnmt* are described in (Harms et al., 2014).

Supplemental References

Balcke, G.U., Kolle, S.N., Kamp, H., Bethan, B., Looser, R., Wagner, S., Landsiedel, R., and van Ravenzwaay, B. (2011). Linking energy metabolism to dysfunctions in mitochondrial respiration--a metabolomics in vitro approach. Toxicology letters 203, 200-209.

Berry, R., and Rodeheffer, M.S. (2013). Characterization of the adipocyte cellular lineage in vivo. Nature cell biology 15, 302-308.

Cohen, P., Levy, J.D., Zhang, Y., Frontini, A., Kolodin, D.P., Svensson, K.J., Lo, J.C., Zeng, X., Ye, L., Khandekar, M.J., Wu, J., Gunawardana, S.C., Banks, A.S., Camporez, J.P., Jurczak, M.J., Kajimura, S., Piston, D.W., Mathis, D., Cinti, S., Shulman, G.I., Seale, P., and Spiegelman, B.M. (2014). Ablation of PRDM16 and beige adipose causes metabolic dysfunction and a subcutaneous to visceral fat switch. Cell 156, 304-316.

Fasshauer, M., Klein, J., Kriauciunas, K.M., Ueki, K., Benito, M., and Kahn, C.R. (2001). Essential role of insulin receptor substrate 1 in differentiation of brown adipocytes. Molecular and cellular biology 21, 319-329.

Harms, M.J., Ishibashi, J., Wang, W., Lim, H.W., Goyama, S., Sato, T., Kurokawa, M., Won, K.J., and Seale, P. (2014). Prdm16 is required for the maintenance of brown adipocyte identity and function in adult mice. Cell metabolism 19, 593-604.

Townsend, M.K., Clish, C.B., Kraft, P., Wu, C., Souza, A.L., Deik, A.A., Tworoger, S.S., and Wolpin, B.M. (2013). Reproducibility of Metabolomic Profiles among Men and Women in 2 Large Cohort Studies. Clinical chemistry 59, 1657-1667.

Walden, T.B., Hansen, I.R., Timmons, J.A., Cannon, B., and Nedergaard, J. (2011). Recruited versus nonrecruited molecular signatures of brown, "brite" and white adipose tissues. Am J Physiol Endocrinol Metab.